A Soft Wearable and Full Textile Piezoresistive Sensor for Plantar Pressure Capturing

Yongsong Tan
Jiangnan University
Kamen Ivanov
Shenzhen Institutes of Advanced Technology Chinese Academy of Sciences
Zhanyong Mei
Chengdu University of Technology
Hui Li
Shenzhen Institutes of Advanced Technology Chinese Academy of Sciences
Ludwig Lubich
Technical University of Sofia
Huihui Li
Shenzhen Institutes of Advanced Technology Chinese Academy of Sciences
Chaoxia Wang
Jiangnan University
lei wang (wang.lei@siat.ac.cn)
Shenzhen Institutes of Advanced Technology Chinese Academy of Sciences

Nano Express

Keywords: textile piezoresistive sensor (TPRS), rGO-cotton fabric electrode, Ag fabric circuit electrode, insole, dynamic plantar pressure

Posted Date: December 1st, 2020

DOI: https://doi.org/10.21203/rs.3.rs-115752/v1

Abstract

The trends of health wearable monitoring system have led to growing demands for gait capturing device. The comfortability and durability under repeated stress in the existing sensor-enabled footwear are still problems. Herein, a flexible textile piezoresistive sensor (TPRS) consisting of rG-cotton fabric electrode and Ag fabric circuit electrode is prepared. Based on the mechanical and electrical properties of two fabric electrodes, the TPRS exhibits superior sensing performance, which includes high sensitivity of 3.96kPa^{-1} in the lower pressure range of 0-36kPa, wide force range (0-800 kPa), fast response time (170 ms), remarkable durability stability (1000 cycles) and dection ability in differrent pressures. For practical application of capturing plantar pressure, six TPRSs are mounted on a flexible printed circuit board and integrated into an insole. The dynamic plantar pressure distribution is displayed through drawing the pressure maps during walking. The proposed full textile piezoresistive sensor is a strong candidate for next-generation plantar pressure wearables monitoring device.

1. Introduction

Flexible wearable device, an unobtrusive sensing interface with the human body, has already become a key tool for capturing human physiological parameters[1-4]. Recently，the trend of flexible wearable device has been focused on improving the performance of softness, breathability and stability[5]. Textiles have become an ideal substrate material for flexible wearable devices due to their high extensibility, easy processing, and low cost [6]. Especially, cotton textiles with large contact surfaces and excellent mechanical properties are introduced to build flexible sensing systems that are comfortable for the wearer [7]. These advantages play key roles in the performance of capturing human information when integrated to a full wearable monitoring device. As a result, a significant number of flexible textile devices with high sensitivity and biocompatibility with skin have been designed for capturing the human movement [8-11]. As piezoresistive pressure sensors are associated with simple preparation process, they possess tremendous potential for wearable device applications [12-17]. For instance, an ultrasensitive fiber-based piezoresistive sensor that can be used to observe the walking signal was fabricated [18].

Wearable plantar pressure capturing system is one of the candidates that greatly benefit from the textile piezoresistive pressure sensors. Analysis of dynamic plantar pressure patterns are used to early alarm and prevention of foot deformities or discovery and rehabilitation monitoring in the advanced stages [19, 20]. The timely detection of abnormal pressures can prevent the development of diabetes ulcers for diabetic [21, 22]. Also, deviations in gait dynamics could indicate the progression of dementia development [23]. Traditional systems for capturing plantar pressure include force plates and pressure sensing walkways [24]. However, the use of these devices is limited to laboratory settings, which makes them unsuitable for continuous monitoring [25-28]. Hence, active engineering and research efforts have been devoted to realize capturing plantar pressure continuously. Sensing insoles can detect dynamic pressure patterns under the main weight-bearing locations of the foot [29-32]. Even though these systems can reflect the dynamic plantar pressure accurately enough, many of them are not biocompatible with the human skin, and easily deform under repeated external pressure, which restricts their application in gait

monitoring [33-35]. Hence, the growing trend of wearable system allow continuous monitoring of plantar pressure patterns, and does not affect the comfort of wearing at the same time.

In the present work, we aim to design a flexible, yet mechanical and electrical stable full textile piezoresistive sensing device with a monitoring system for capturing plantar pressure. Here, the cotton fabric, a basic wearable material with the characteristics of softness, breathability and high conformability, is designed as the substrate to construct the fabric electrode. The rGO-cotton fabric electrode and Ag fabric circuit electrode demonstrate a high conductivity of 16.3 kΩ/cm and 0.5 Ω/cm. With the help of rGO and Ag, the TPRS with high flexibility and durability endowed by fabric electrode shows high sensitivity of 3.96kPa^{-1} in the lower pressure range of 0-36kPa, wide force range (0-800 kPa), fast response time (170 ms) and remarkable durability stability (1000 cycles). To illustrate the use of the proposed TPRS in capturing plantar pressure, six TPRSs are mounted on a flexible printed circuit board that is attached to the textile part of a commercial insole to form a complete sensor device for monitoring the plantar information. The device is connected to a custom electronic acquisition module, and its capability to reflect plantar pressure is proved. The provided pressure distribution performance results of gait capturing indicate that the textile flexible piezoresistive sensor has tremendous application potential in wearable device.

2. Experimentation

2.1 Materials and reagents

The graphene oxide (GO) was purchased from Suzhou Crystal Silicon Electronice & Technology Co, Ltd, china. The Ag paste and sodium hyposulfite were purchased from aladin. All reagents were of analytical grade and used as received without further purification.

2.2 Fabrication of rGO-cotton fabric electrode

To enhance the interface adsorption of cotton fabric, the fabric electrode was treated with oxygen plasma. The pretreated cotton fabric was prepared by cleaning the fabric with deinonized water to remove the impurities, after that the cleaned fabric was treated with oxygen plasma for 5min. And the rGO cotton fabric electrode was prepared by repeatedly impregnating and reduction. The fabric was immersed in 3 mg/ml GO in deionized water solution for 15 min and dried in an oven at 80°C for 30 min. After repeating this process three times, the GO on the surface of the cotton was reduced to rGO in sodium hyposulfite solution (10g/L) at 90°C for 8h.

2.3 Fabrication of Ag fabric circuit electrode

A mask was formed in the PI tape covering the surface of the cotton fibres using a laser cutting machine. The unnecessary cut part of the PI tape was removed using tweezers to obtain the fabric electrode circuit. After treatment with oxygen plasma, the circulation circuit was coated with silver paste, and the

conductive circuit was treated in a vacuum drying oven at 70 ℃ for 30 minutes. Then, the conductive fabric circuit was obtained by removing the PI tape.

2.4 Fabrication of the textile piezoresistive sensor

The TPRS was constructed with the conductive rGO cotton fabric electrode and Ag fabric circuit electrode, where the outer surfaces of the both are covered by Polyimide (PI) tape substrate. In addition, the Ag fabric circuit electrode was electrically connected with embedded copper electrode as interconnectors.

2.5 Fabrication of the sensor insole

With a limited number of sensors, the proper selection of sensor positions under the foot is essential [36]. In the insole, six piezoresistive sensors were mounted under the main weight-bearing positions, namely the big toe, first and fourth metatarsal heads, the midfoot and heel. The sensors were first mechanically fixed to the flexible printed circuit board using thin double-sided adhesive tape and were then electrically connected. The sensor surface of the sole was covered with a thin transparent plastic sheet layer that was also sewn to the textile base of a commercial insole. Finally, the complete sensor insole was placed into shoes and connected to the electronic acquisition module.

In order to test the accuracy in reflecting the pressure change, a commercial reference sensor has been introduced for comparison with TPRS during walking. For that, each reference sensor was carefully aligned on the top surface of its corresponding TPRS.

2.6 Characterizations

The SEM was used to investigated the morphology of fabric electrode. The swatches were coated with a 5-10 nm Au layer before the SEM imaging. A Keithley 2400 source/meter (4-wire) was employed to measure the resistance of rGO cotton fabric electrode, Ag fabric circuit electrode. The pressure was applied to the TPRS using the universal testing machine (AG-X plus, Shimadzu, Japan), and the resistance of TPRS was tested using Keithley 2400 source/meter (4-wire). Before applying the pressure on the TPRS, a cube (10mm× 10 mm) was designed to placed on the contact area.

3. Results And Discussion

Figure 1 demonstrates the fabrication process and structure of TPRS. The TPRS comprises the conductive rGO-cotton fabric electrode (Fig1.b) and the Ag fabric circuit electrode (Fig1.c), in which the outer surfaces of the both are covered by Polyimide (PI) tape substrate, as shown in 1a. And the TPRS are assembled in different positions to obtain the insole which can monitor the gait information, as shown in Fig 1d. Fig 1e-g show digital photographs of the insloe, encapsulated insole and smart shoe. A detailed fabrication process of the TPRS is presented in the Experimental section.

Figure 2 shows the SEM images of morphology of the rGO-cotton electrode and the Ag fabric circuit electrode. Compared with the control cotton fabric (Fig 2a), a uniform coating layer of silver paste was

formed on the surface of cotton fabric, as shown in Fig 2b. And the surface resistance of Ag fabric circuit electrode is 0.5Ω/cm, which can be attributed to the excellent conductivity of silver paste. To be noticed, the reduced graphene oxide (rGO) is wrapped on the surface on the surface of cotton yarns, as shown in Fig 2c-d. The surface resistance of rGO fabric electrode is 16.3KΩ/cm.

The sensing mechanism of TPRS is explained with the change in the resistance of the contact between the rGO-cotton electrode and the fabric circuit one upon the application of pressure over the outer sensor surfaces. Increasing pressure leads to the formation of small compressive deformations that enhance the contact between the two conductive fabrics and reduces the interlayer distance between them. Thus also, the number of electrical pathways between the two electrodes increases. With small forces, the decrease in resistance is small, while it becomes evident at higher pressures. Also, upon initial contact between the two electrode parts, the resistance of the sensor decreases rapidly, while this decrease becomes gradual upon reaching full contact between the surfaces of the electrodes. This behavior of change of the sensor resistance is explained with the fact that the graphene sheets are stacked together to form a graphite-like bulk body, which accelerates charge hopping between the overlapping graphene islands [37]. When high pressure is applied to the TPRS, charge hopping occurs between the overlapping graphene islands. After unloading the pressure, the TPRS recovers its initial shape, which results in decreasing the contact area and less electrical pathways. The changes of resistance upon the application of different pressures is also thoroughly tested.

In this study, the sensing performance of the TPRS is assessed in terms of normalized resistance change, response time, stable durability and dynamic response. A computer-controlled force gauge platform and an electrical signal analyzer are used to test the dynamic characteristics under different test models. To invetigate the performance of TPFS, the relative current changes ($\Delta I/I_0$) versus pressure is showned in Fig 3a. And the sensitivity of the TPFS is 3.96kPa^{-1} in the lower pressure range of 0-36kPa while the sensitivity lowers to 0.49 kPa^{-1} in higher pressure range. This performance of TPFS in different pressure range is consistent with the results discussed above. Fig 3b shows the relative resistance change of full textile piezoresistive sensor under a pressure of 5 KPa. In this case, the TPFS shows the stable resistance response, excellent repeatability and durability. The response and recovery time of TPRS are 170 ms and 261 ms, respectively, as shown in Fig 3d-e. Interestingly, the releasing time for higher pressure is much longer. Under a larger force, the rGO cotton fabric electrode and Ag fabric circuit electrode are in close contact, and recovery needs a longer time. It is worth emphasizing that the primary goal in the design is to obtain a wearable full textile sensor that accurately reflects plantar pressure changes rather than pursuing fast response times.

In order to verify the adaptability of TPRS to varying plantar pressure and stability to repeated pressure cycles, cyclic force (including loading and unloading process) between 0 and 80 N at a speed of 20 mm/min with 5s pause is applied to the TPRS. It is important for the TPRS to have excellent recovery characteristics to ensure stable performance and a long lifetime. The durability performance along the repeated cycles is illustrated in Fig 4a. Due to the excellent recovery characteristics of the cotton fabric, the TPRS resistance returns to its initial value after unloading the pressure. The phenomenon of signal

drift and structural damage are not significant during the load/release cycles due to the excellent mechanical and electrical properties of the cotton fabric electrodes. As shown in Fig 4b-d, the resistance value of TPFS fluctuated at the moment of loading and releasing the pressure. In the whole cycle, the inherent elasticity of the fabric electrode makes it difficult for the two fabric electrodes to response quickly to the external pressure, which brings about a delay of resistance variation. Interstingly, we observe that the resistance of the TPFS has a jump and then chang rapidly as the pressure increases, as shown in yellow area of Fig 4b-d. This can be explained by the contact resistance changed between rGO cotton fabric electrode and Ag fabric circuit electrode upon the application of pressure over the outer sensor surfaces. At the beginning, the resistance of the TPRS decreases suddenly when the two fabric electrodes first contact. The increasing pressure leads to the formation of small compressive deformations that enhance the contact point between the two conductive fabrics and reduces the interlayer distance between them. For capturing plantar pressure, the sensor needs to have a high sensitivity and this ability is also tested, as shown in Fig 5a. There is obvious resistancechange under varying pressure with high sensitivity. It can be seen that the TPRS is more sensitive in a smaller pressure range, but less sensitive to pressure in a larger pressure range. And the TPRS is capable of operating up to the pressure of 800 kPa before failure (Fig S1). The sensor shows high sensitivity to the external stimulus under the pressures as high as 800 kPa that are typical for plantar pressure measurements.

In order to interpret the relationship between current and voltage, pressure and current, and pressure and resistance, a circuit are designed. And one of the benefits of the transimpedance amplifier circuit is that it maintains a constant voltage over the sensor, thus avoiding influence of eventual non-linearities of the voltage-current characteristic of the sensor. As the reciprocal slope of the straight line represents the resistance of the TPFS based on $R=V/I$, the current and voltage of the sensor are linear when the resistance is constant. As shown in Fig 5b, the current almost increase linearly with the applied voltage and the slope of the line did not change at the same pressure. When the constant voltage applied to the TPFS, the current through the sensor increases correspondingly with the pressure increase. The resistance will decrease when pressure is applied, resulting in an increase in the current ($I=V/R$). And the slope of lines (Slope=I/V) will increase with the increase of pressure applied in TPFS, indicating that the resistance value of TPFS decreases with the pressure increasing. It indicates that the TPRS exhibits high resistance sensitivity and a high linear relationship between pressure and resistance.

Different pressure points under the foot can reflect gait information. If the force points of the TPRS are selected not properly, the correct gait information will not be detected [36]. Here, we demonstrated a wireless wearable plantar pressure capturing device that employed our proposed textile piezoresistive sensor. In the fabrication of insole for capturing plantar information, six piezoresistive sensors are mounted under the main weight-bearing positions named as “big toe”, “methatarsal 1”、“methatarsal 4”, “midfoot”, “heel 1” and “heel 2” respectively. TPRS “big toe” located in the medial upper corner of the insole is employed to detect the pressure mainly under the big toe area. TPRS “methatarsal 1”and “methatarsal 4” located below the big toe are used to detect the pressure under the proximal interphalangeal joint area. TPRS midfoot is located in the metatarsal-phalangeal joint area. And TPRS “heel 1” and “heel 2” are located in the heel area. Here, the proposed insole is configured to collect and

save the data in real time during walking at a comfortable speed. The micro control unit, the circuit board, and the battery are mounted on a wearable shoe, as shown in Fig 1g. The measured TPRS outputs are transferred to a computer via Bluetooth Low Energy v. 5. And the electronic acquisition module is designed to obtain the signals of all insole sensors in real time, as shown in Fig S2. As a result, a wireless monitoring system that can remotely monitor the pressure sensor signals is designed to prevent electrical wires from restricting natural body movements.

A custom commercial sensor has been introduced for comparison with TPRS during walking, as shown in Fig 1f. To ensure the custom sensors and TPRS receive the same pressure during walking, two types of sensors are placed at the same point, where the custom sensor is top on the surface of the TPRS. As shown in Fig 6, both TPRS and the custom sensor can accurately distinguish and react to the changes in pressure during walking. The TPRS and the custom sensor appear under the same external force exhibited obvious response difference. The change of TPRS is more intuitive and obvious after being subjected to external force, which makes the fabric sensor more suitable for the collection of human foot information.

In addition, for verifying the response of TPRS on the smart insole to external pressure accurately, the calibration procedures (Fig S3) of TPRS are carried out. In order to demonstrate the excellent performance of smart insole for gait recognition, a healthy adult volunteer with a weight of 60 kg is invited to wear the fiber-based smart insole. The volunteer wear comfortable sportswear and athletic shoes equipped with pressure-sensitive foot insole and is asked to walked over a 100 m at self-selected speed for some minutes to become familiarized with the equipment. The 5 times data of plantar pressure changes during walking are collected and analyzed. In particular, subject is requested to repeat the ground-level walking task for 5 times at a self-selected slow speed, and for 5 times at a self-selected normal speed. The resistance change of the TPRS in different parts of the insole during walking is shown in Fig7. Fig 7 clarifies the experimental setup and the gait cycles reflected by the signals collected from the insole.

The ground contact is initiated by the heel strike and reflected by the highest amplitude of “heel 1” and “heel 2” sensor signals. Then, foot flat phase is reflected by the relatively low-amplitude signal of the midfoot sensor. Finally, the signals of the metatarsal sensors and the big toe sensor denote the end of the ground contact. After obtaining the plantar pressure data, we analyze the pressure distribution of smart insole and drawn the distribution of the plantar pressure when walking, as shown in Figure 8. The gait signal is smoothed and noise is removed. In the process of five situations: feet off the ground, feet start to land, feet on the ground, feet start to get off the ground, feet off the ground, the pressure distribution of the corresponding part of the insole will also change accordingly. Normally, the heel first contacts, followed by the midfoot, the forefoot, and then toe pressure. As shown in Fig 8a-i, a complete pressure distribution diagram (see details in supporting information Figure movie S1) is shown from the foot touching the ground to the foot leaving the ground. First, the plantar pressure distribution demonstrates that the plantar pressure basically does not change when the foot is lifted during walking, as shown in Fig 8a. And the pressure on the insole changes in the order of “heel 1” and “heel 2” (as shown in Fig 8b),

“midfoot” (as shown in Fig 8c), “metatarsal 1” and “methatarsal 4” (as shown in Fig 8e) respectively when the foot begins to touch the ground. Then, the pressure at each part of the sole reaches the maximum value when the foot is in full contact with the ground, as shown in Fig 8e. Next, Fig 8f-h shows the pressure distribution change of smart insole after the foot starts to leave the ground. Finally, the insole is basically free of force when the foot leaves the ground, as shown in Fig 8i. Judging from the pressure distribution of plantar pressure, the pressure of “methatarsal 4” is higher than other parts when walking. In contrast, the pressure on “midfoot” received the minimal pressure. Our proposed sensor may be employed to feedback gait information and to assess health status for both hemiparetic patients and healthy individuals. These results demonstrated that the proposed insole is suitable for real time gait recognition in various environments.

Conclusion

In summary, we design a novel wearable piezoresistive sensor based on excellent mechanical and electrical properties of two kinds of fabric electrodes for capturing plantar pressure. And the smart insole is success fully prepared by mounting TPRS into six different points on each insole. The TPRS demonstrated high sensitivity of 3.96kPa^{-1} in the lower pressure range of 0-36kPa in a wide pressure range (0-800 kPa), outstanding response to external pressure, stable durability (1000 cycles) and fast response time (170 ms) confirming its potential for real-time detecting human movement. And the develop monitoring insloe takes advantage of high sensitivity, high resolution under different pressure and excellent durability, which allows stable plantar signals under different contact pressure. The analysis of pressure distributions under the foot sole can be evaluated by drawing the pressure maps in different gait phases. The proposed TPRS holds a promise for e-skin and other wearable sensing applications.

Declarations

Conflicts of interest

The authors declare no conflict of interest.

Acknowledgments

This study was supported by the National Key Research and Development Program of China (2018YFC2000903), National First-Class Discipline Program of Light Industry Technology and Engineering (LITE2018-21), National Natural Science Foundation of China (21975107) and by Fundamental Research Funds for the Central Universities (JUSRP51724B), Key Project 2017GZ0304 of the Science and Technology Department of Sichuan province and the young and middle-aged backbone teachers’ program of Chengdu University of Technology, the Shenzhen-Hong Kong Institute of Brain Science–Shenzhen Fundamental Research Institutions (NYKFKT2020002).

References

[1] S Wang, JY Oh, J Xu, H Tran, Z Bao (2018) Skin-Inspired Electronics: An Emerging Paradigm. Accounts of Chemical Research: acs.accounts.8b00015. http://doi.org/Doi:10.1021/acs.accounts.8b00015

[2] Y Wang, W Li, Y Zhou, et al. (2020) Fabrication of high-performance wearable strain sensors by using CNTs-coated electrospun polyurethane nanofibers. Journal of Materials Science 55: 12592-12606. http://doi.org/Doi:10.1007/s10853-020-04852-8

[3] T Xie, Q Liu, G Xue, X Gou (2020) Numerical analysis of piezoelectric and mechanical response of buckled poly(vinylidene fluoride) nanofibers for the design of highly stretchable electronics. Journal of Materials Science 55: 10668-10677. http://doi.org/Doi:10.1007/s10853-020-04791-4

[4] Y Wu, W Xu, JJ Liu, M-C Huang, S Luan, Y Lee (2014) An energy-efficient adaptive sensing framework for gait monitoring using smart insole. IEEE Sensors Journal 15: 2335-2343. http://doi.org/Doi:10.1109/JSEN.2014.2372694

[5] Thanh-Giang, La, Shide, et al. (2018) Two-Layered and Stretchable e-Textile Patches for Wearable Healthcare Electronics. Advanced Healthcare Materials. http://doi.org/Doi:10.1002/adhm.201801033

[6] LM Castano, AB Flatau (2014) Smart fabric sensors and e-textile technologies: a review. Smart Materials and Structures 23: 053001. http://doi.org/Doi:10.1088/0964-1726/23/5/053001

[7] Y Li, X Miao, RK Raji (2019) Flexible knitted sensing device for identifying knee joint motion patterns. Smart Materials and Structures 28: 115042. http://doi.org/Doi:10.1088/1361-665X/ab4afe

[8] CL Choong, MB Shim, BS Lee, et al. (2014) Highly stretchable resistive pressure sensors using a conductive elastomeric composite on a micropyramid array. Advanced materials 26: 3451-3458. http://doi.org/Doi:10.1002/adma.201305182

[9] M Liu, X Pu, C Jiang, et al. (2017) Large-Area All-Textile Pressure Sensors for Monitoring Human Motion and Physiological Signals. Adv Mater 29. http://doi.org/Doi:10.1002/adma.201703700

[10] T Yang, D Xie, Z Li, H Zhu (2017) Recent advances in wearable tactile sensors: Materials, sensing mechanisms, and device performance. Materials Science and Engineering: R: Reports 115: 1-37. http://doi.org/Doi: 10.1016/j.mser.2017.02.001

[11] N Forintos, T Czigany (2020) Reinforcing carbon fibers as sensors: The effect of temperature and humidity. Composites Part A: Applied Science and Manufacturing 131: 105819. http://doi.org/Doi:10.1016/j.compositesa.2020.105819

[12] TT Tung, MJ Nine, M Krebsz, et al. (2017) Recent advances in sensing applications of graphene assemblies and their composites. Advanced Functional Materials 27: 1702891. http://doi.org/Doi:10.1002/adfm.201702891

[13] W Wu, X Wen, ZL Wang (2013) Taxel-addressable matrix of vertical-nanowire piezotronic transistors for active and adaptive tactile imaging. Science 340: 952-957. http://doi.org/Doi:10.1126/science.1234855

[14] W Zeng, L Shu, Q Li, S Chen, F Wang, XM Tao (2014) Fiber-based wearable electronics: a review of materials, fabrication, devices, and applications. Adv Mater 26: 5310-5336. http://doi.org/Doi:10.1002/adma.201400633

[15] S Gong, W Schwalb, Y Wang, et al. (2014) A wearable and highly sensitive pressure sensor with ultrathin gold nanowires. Nat Commun 5: 3132. http://doi.org/Doi:10.1038/ncomms4132

[16] DJ Lipomi, M Vosgueritchian, BC Tee, et al. (2011) Skin-like pressure and strain sensors based on transparent elastic films of carbon nanotubes. Nat Nanotechnol 6: 788-792. http://doi.org/Doi:10.1038/nnano.2011.184

[17] X Wang, Y Gu, Z Xiong, Z Cui, T Zhang (2014) Silk-molded flexible, ultrasensitive, and highly stable electronic skin for monitoring human physiological signals. Adv Mater 26: 1336-1342. http://doi.org/Doi:10.1002/adma.201304248

[18] M Cao, M Wang, L Li, H Qiu, MA Padhiar, Z Yang (2018) Wearable rGO-Ag NW@ cotton fiber piezoresistive sensor based on the fast charge transport channel provided by Ag nanowire. Nano energy 50: 528-535. http://doi.org/Doi:10.1016/j.nanoen.2018.05.038

[19] Z Mei, K Ivanov, G Zhao, H Li, L Wang (2017) An explorative investigation of functional differences in plantar center of pressure of four foot types using sample entropy method. Medical & biological engineering & computing 55: 537-548. http://doi.org/Doi:10.1007/s11517-016-1532-7

[20] Z Mei, G Zhao, K Ivanov, et al. (2013) Sample entropy characteristics of movement for four foot types based on plantar centre of pressure during stance phase. BioMedical Engineering OnLine 12: 101. http://doi.org/Doi:10.1186/1475-925x-12-101

[21] Z Pang, G Yang, R Khedri, Y Zhang (2018) Introduction to the Special Section: Convergence of Automation Technology, Biomedical Engineering, and Health Informatics Toward the Healthcare 4.0. IEEE Reviews in Biomedical Engineering 11: 249-259.

[22] W Tao, T Liu, R Zheng, H Feng (2012) Gait analysis using wearable sensors. Sensors (Basel, Switzerland) 12: 2255-2283. http://doi.org/Doi:10.3390/s120202255

[23] J Verghese, RB Lipton, CB Hall, G Kuslansky, MJ Katz, H Buschke (2002) Abnormality of gait as a predictor of non-Alzheimer's dementia. The New England journal of medicine 347: 1761-1768. http://doi.org/Doi:10.1056/NEJMoa020441

[24] S Urry (1999) Plantar pressure-measurement sensors. Measurement Science and Technology 10: R16. http://doi.org/Doi:10.1088/0957-0233/10/1/017

[25] AL Adkin, JS Frank, MG Carpenter, GW Peysar (2000) Postural control is scaled to level of postural threat. Gait & posture 12: 87-93. http://doi.org/Doi:10.1016/S0966-6362(00)00057-6

[26] MN Orlin, TG McPoil (2000) Plantar pressure assessment. Physical therapy 80: 399-409. http://doi.org/Doi:10.1016/S0030-5898(05)70151-6

[27] SC Wearing, SR Urry, JE Smeathers (2000) The effect of visual targeting on ground reaction force and temporospatial parameters of gait. Clinical biomechanics 15: 583-591. http://doi.org/Doi:10.1016/S0268-0033(00)00025-5

[28] DA Winter (1991) The biomechanics and motor control of human gait: Normal, elderly, and pathological. JOURNAL OF REHABILITATION RESEARCH AND DEVELOPMENT

[29] S Crea, M Donati, SM De Rossi, CM Oddo, N Vitiello (2014) A wireless flexible sensorized insole for gait analysis. Sensors (Basel) 14: 1073-1093. http://doi.org/Doi:10.3390/s140101073

[30] W Heng, G Pang, F Xu, X Huang, Z Pang, G Yang (2019) Flexible Insole Sensors with Stably Connected Electrodes for Gait Phase Detection. Sensors (Basel) 19. http://doi.org/Doi:10.3390/s19235197

[31] C Wang, Y Kim, H Shin, SD Min (2019) Preliminary Clinical Application of Textile Insole Sensor for Hemiparetic Gait Pattern Analysis. Sensors (Basel) 19. http://doi.org/Doi:10.3390/s19183950

[32] SW Park, PS Das, JY Park (2018) Development of wearable and flexible insole type capacitive pressure sensor for continuous gait signal analysis. Organic Electronics 53: 213-220. http://doi.org/Doi:10.1016/j.orgel.2017.11.033

[33] P Aqueveque, R Osorio, F Pastene, F Saavedra, E Pino (2018) Capacitive Sensors Array for Plantar Pressure Measurement Insole fabricated with Flexible PCB. Conf Proc IEEE Eng Med Biol Soc 2018: 4393-4396. http://doi.org/Doi:10.1109/EMBC.2018.8513383

[34] AM Ngueleu, AK Blanchette, L Bouyer, et al. (2019) Design and Accuracy of an Instrumented Insole Using Pressure Sensors for Step Count. Sensors 19: 984. http://doi.org/Doi:10.3390/s19050984

[35] L Paredes-Madrid, CA Palacio, A Matute, CA Parra Vargas (2017) Underlying Physics of Conductive Polymer Composites and Force Sensing Resistors (FSRs) under Static Loading Conditions. Sensors (Basel) 17. http://doi.org/Doi:10.3390/s17092108

[36] D Rosenbaum, HP BECKER (1997) Plantar pressure distribution measurements. Technical background and clinical applications. Foot and ankle surgery 3: 1-14. http://doi.org/Doi:10.1046/j.1460-9584.1997.00043.x

[37] MA Mohammad Haniff, S Muhammad Hafiz, KA Wahid, et al. (2015) Piezoresistive effects in controllable defective HFTCVD graphene-based flexible pressure sensor. Sci Rep 5: 14751.

http://doi.org/Doi:10.1038/srep14751

Figures

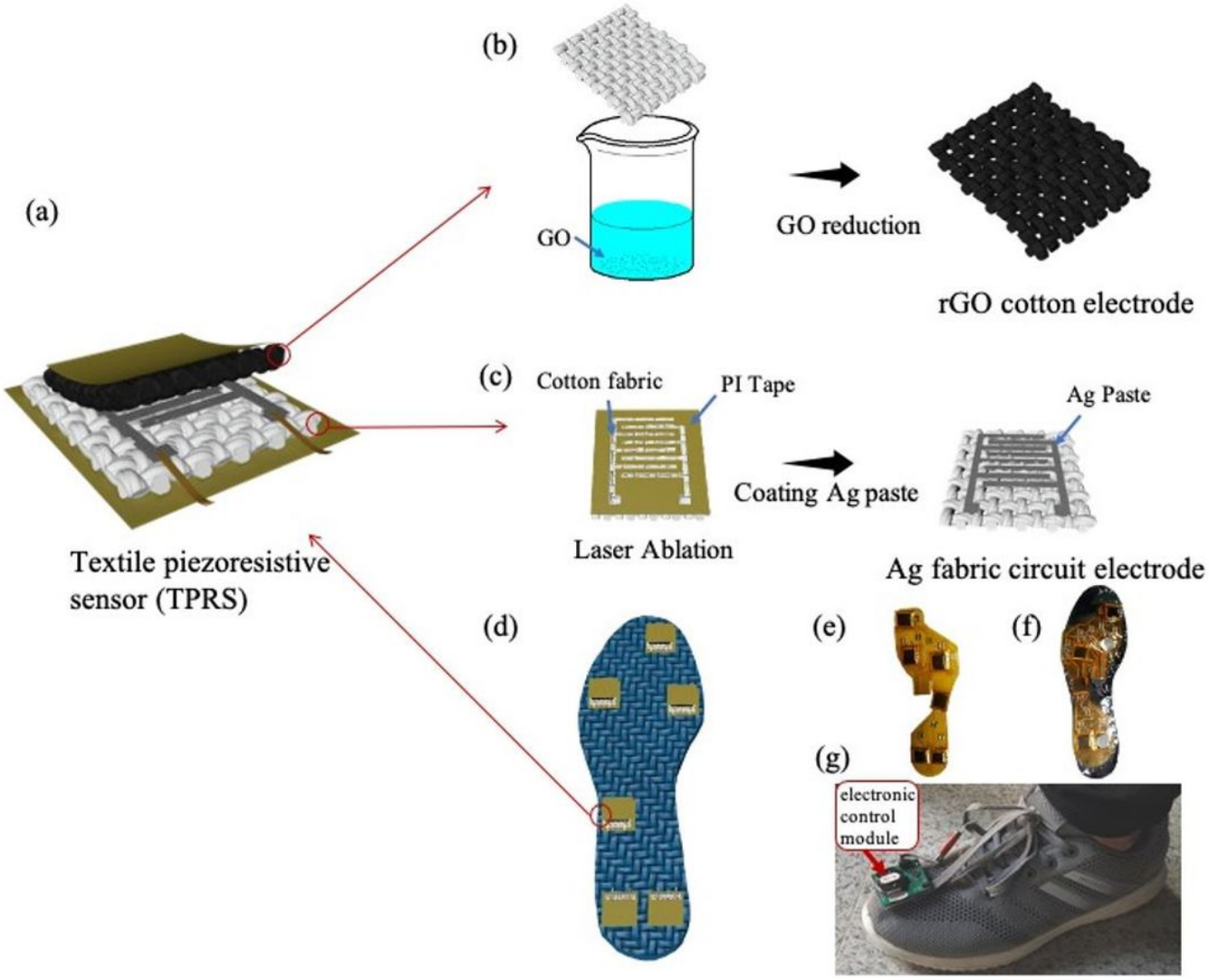

Figure 1

Schematic illustration of fabric electrode and TPRS: (a) The preparation process of the fabric electrode coated with silver paste, (b) The preparation process of the fabric electrode coated with rGO, (c) the assembly process with PI tape, (d) the preparation process of the complete TPRS. Optical images of the (e) the insole, (f) encapsulated insole and (g) smart shoe.

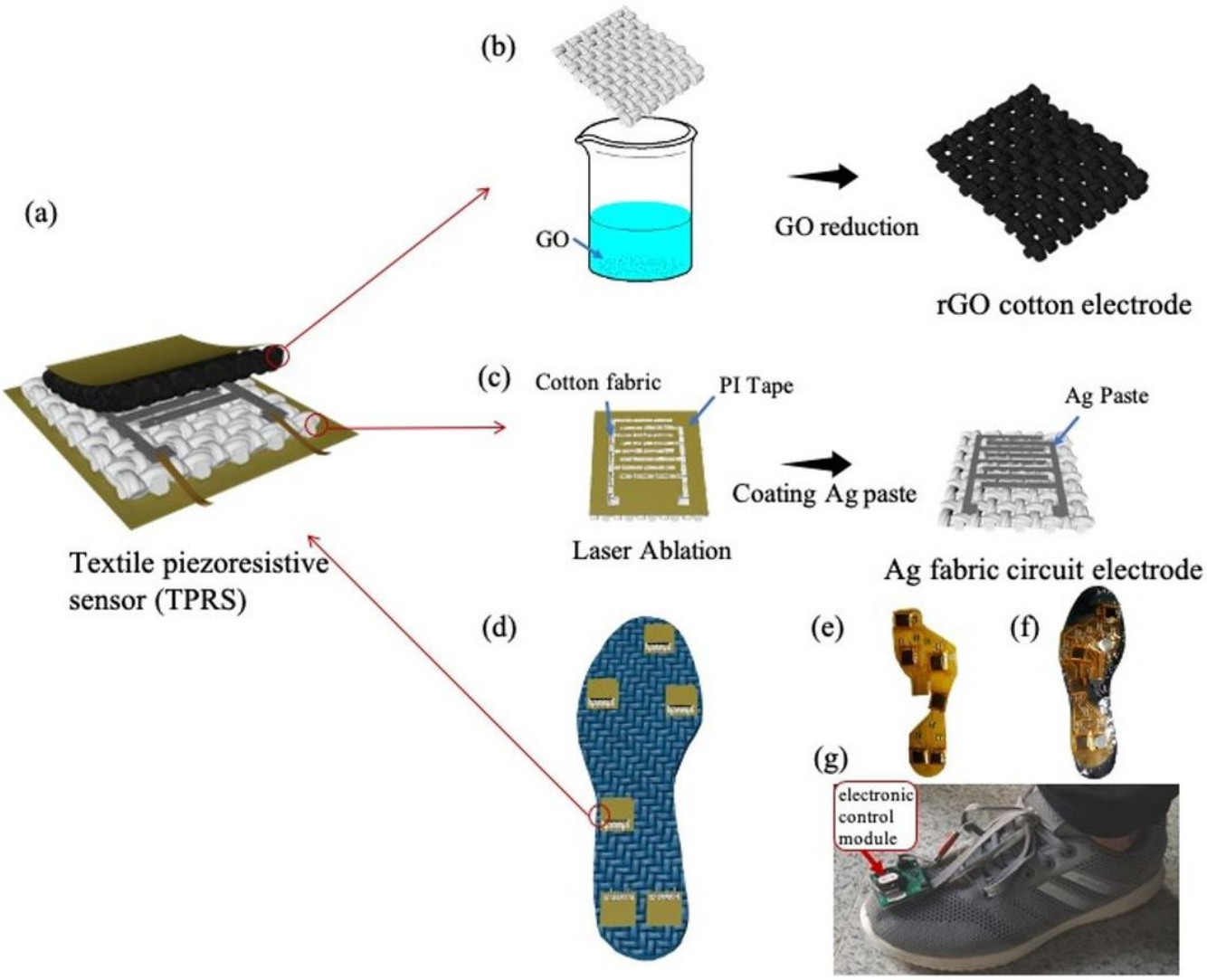

Figure 1

Schematic illustration of fabric electrode and TPRS: (a) The preparation process of the fabric electrode coated with silver paste, (b) The preparation process of the fabric electrode coated with rGO, (c) the assembly process with PI tape, (d) the preparation process of the complete TPRS. Optical images of the (e) the insole, (f) encapsulated insole and (g) smart shoe.

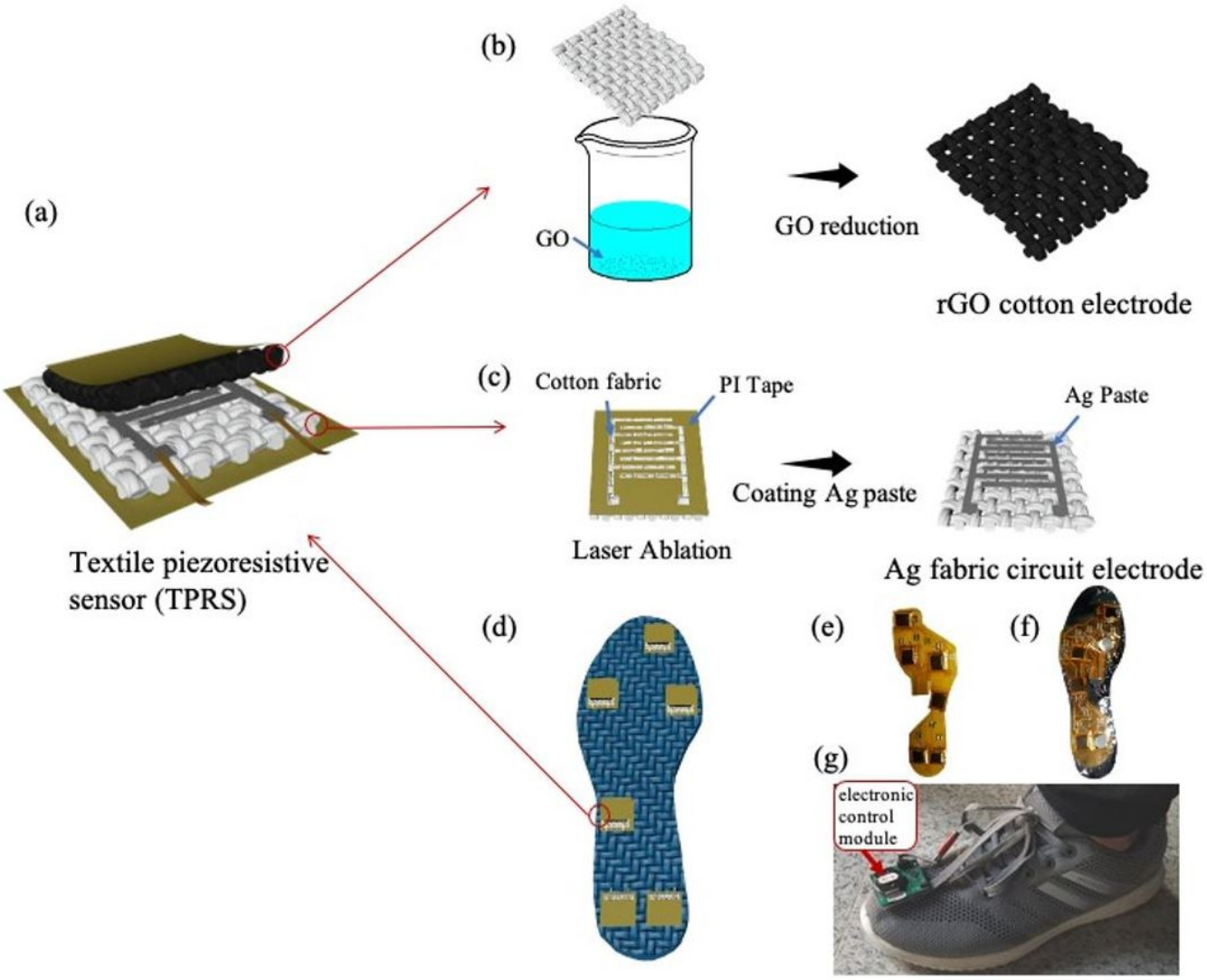

Figure 1

Schematic illustration of fabric electrode and TPRS: (a) The preparation process of the fabric electrode coated with silver paste, (b) The preparation process of the fabric electrode coated with rGO, (c) the assembly process with PI tape, (d) the preparation process of the complete TPRS. Optical images of the (e) the insole, (f) encapsulated insole and (g) smart shoe.

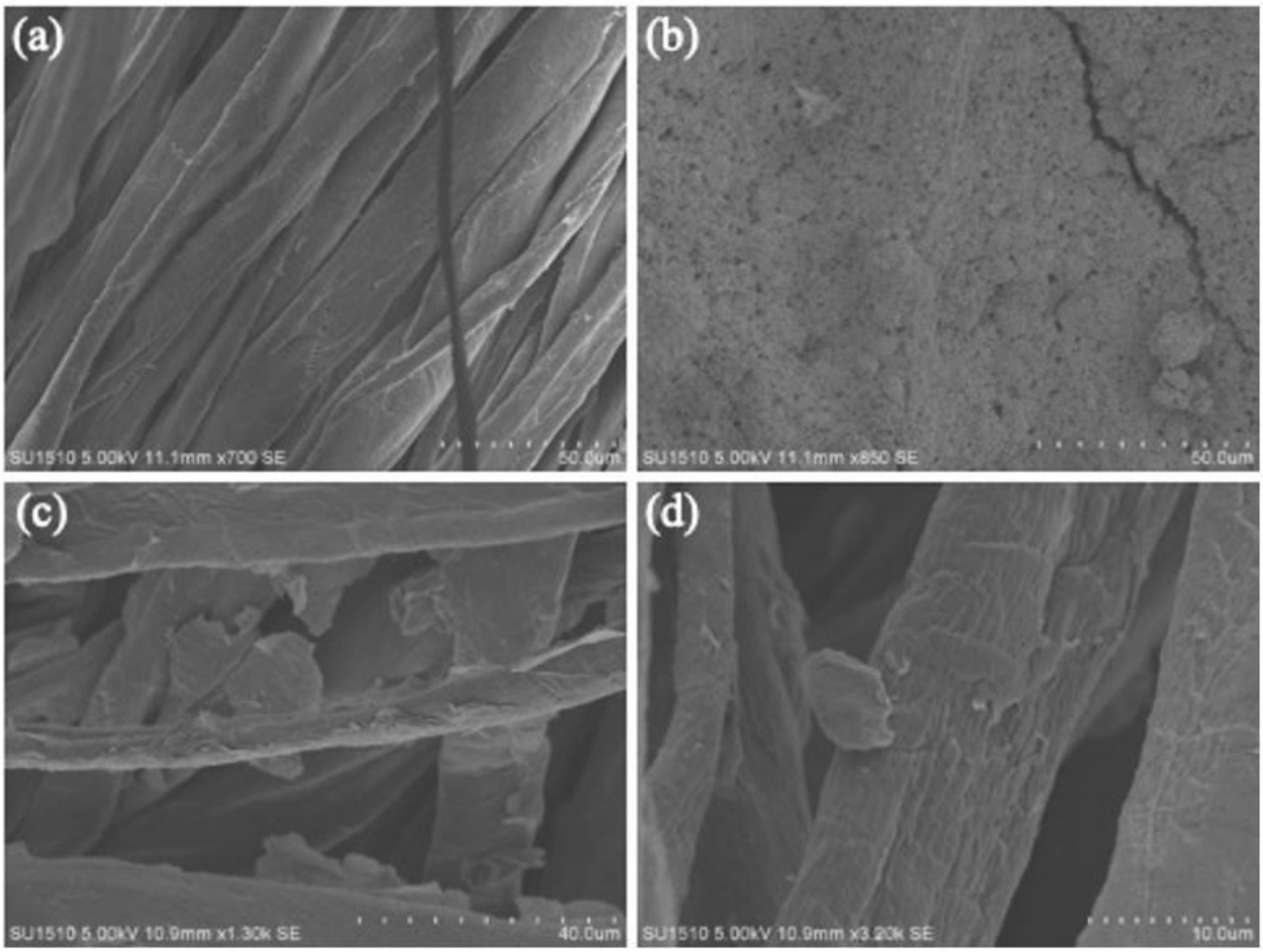

Figure 2

The SEM images of the surface morphology of (a)control cooton fabric, (b) the Ag fabric circuit electrode and (c-d) the rGO-cotton electrode.

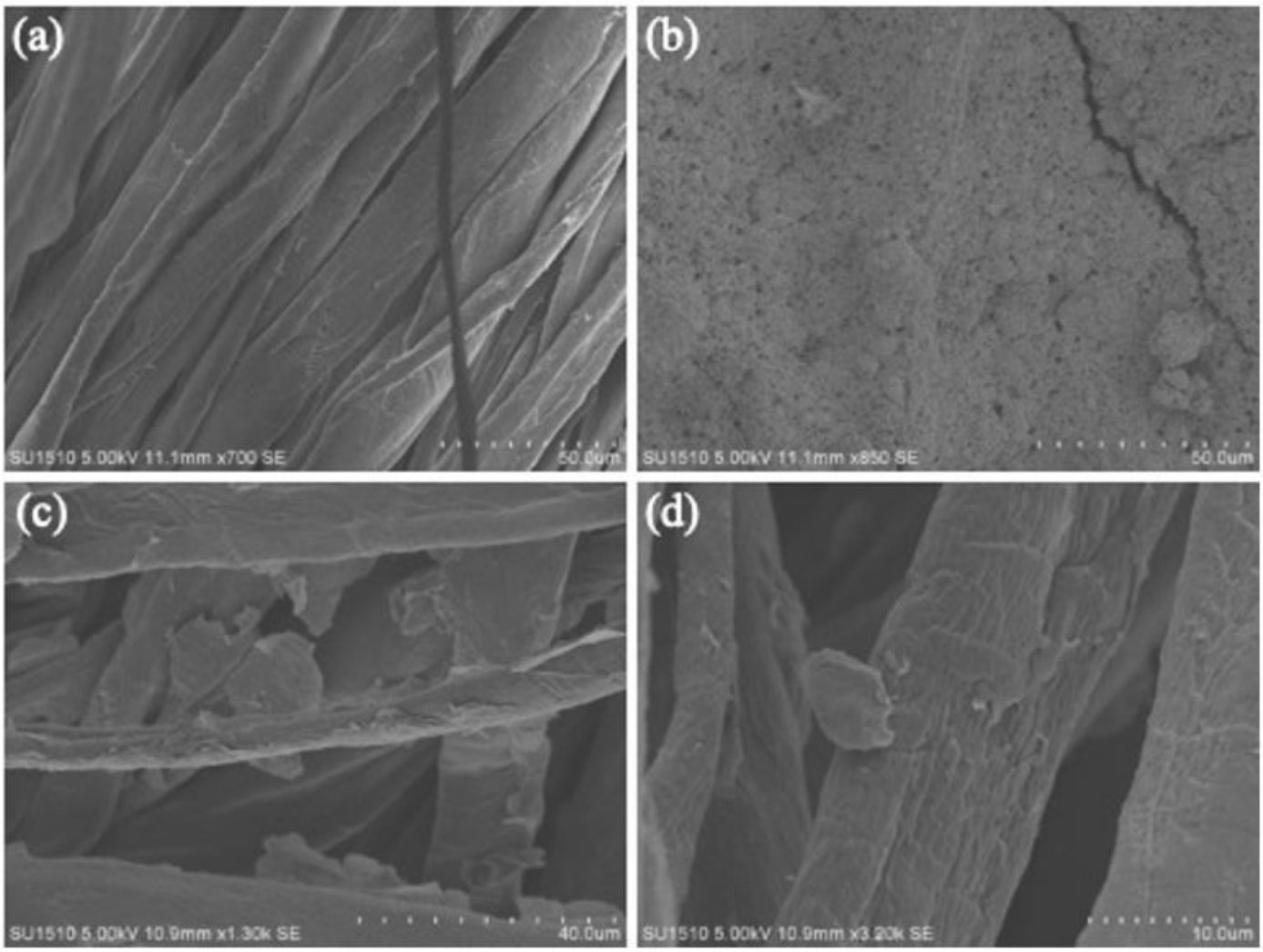

Figure 2

The SEM images of the surface morphology of (a)control cooton fabric, (b) the Ag fabric circuit electrode and (c-d) the rGO-cotton electrode.

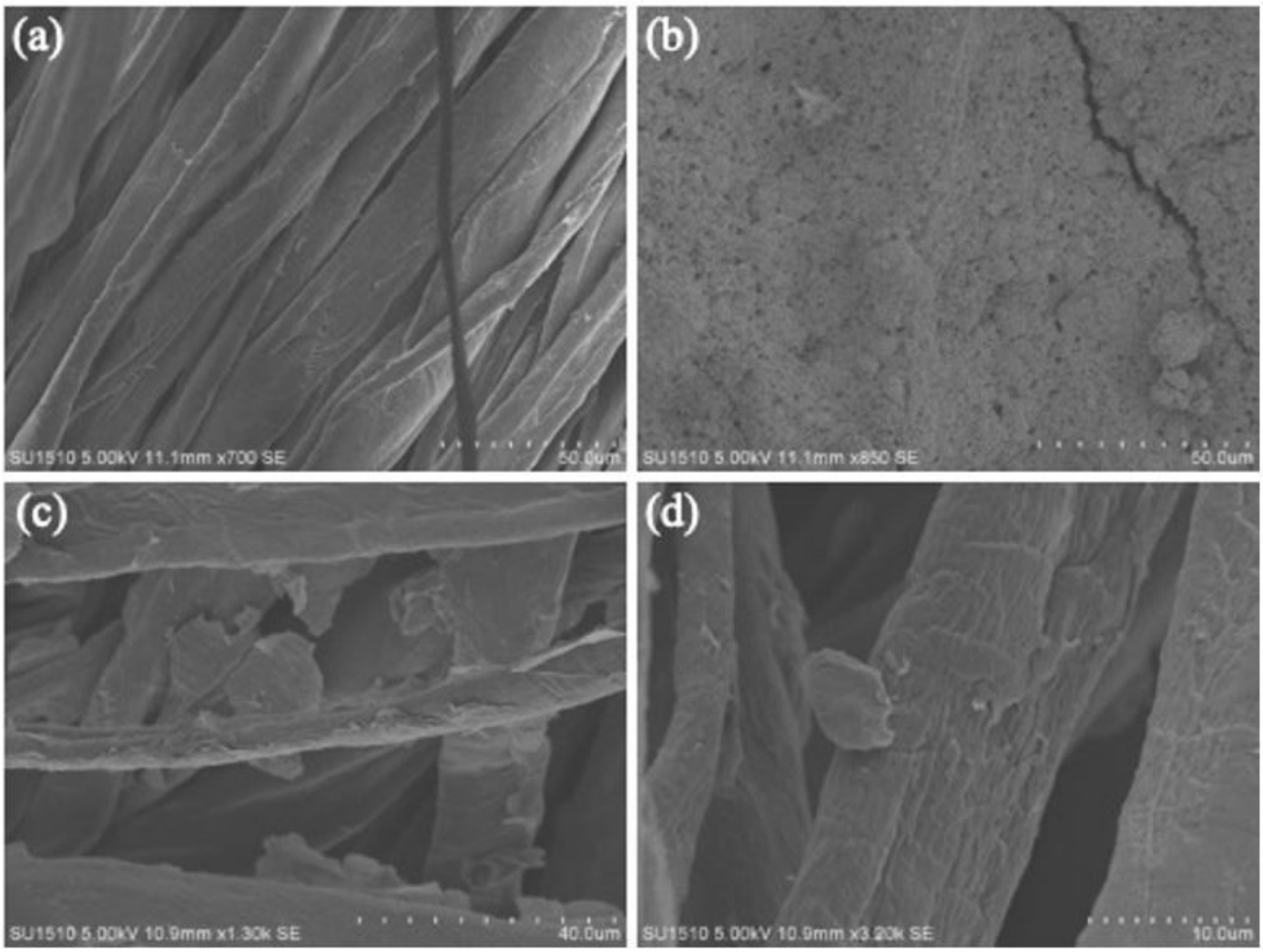

Figure 2

The SEM images of the surface morphology of (a)control cooton fabric, (b) the Ag fabric circuit electrode and (c-d) the rGO-cotton electrode.

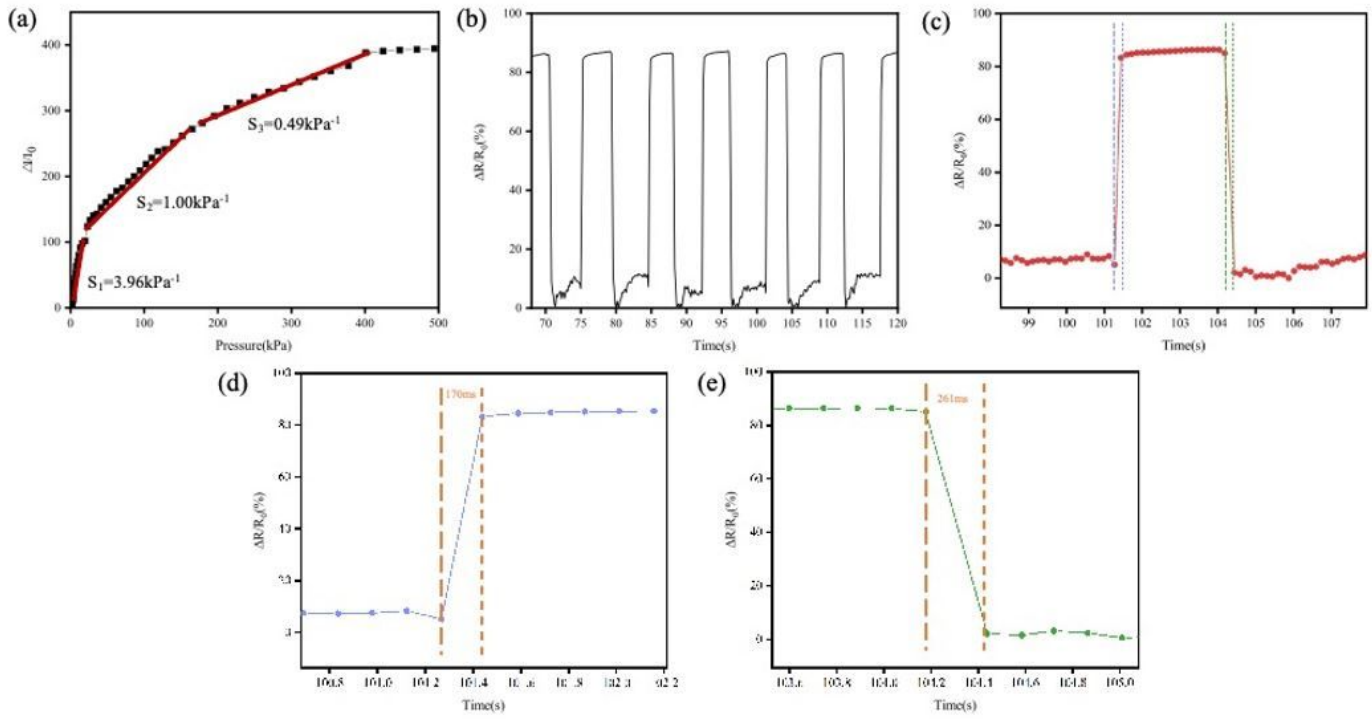

Figure 3

(a) The sensitivity performace of TPRS. (b) Real-time response of the sensor under an applied pressure of 5 KPa. (c) Pressure response showing a single cycle, and the corresponding (d) response time and (e) releasing time.

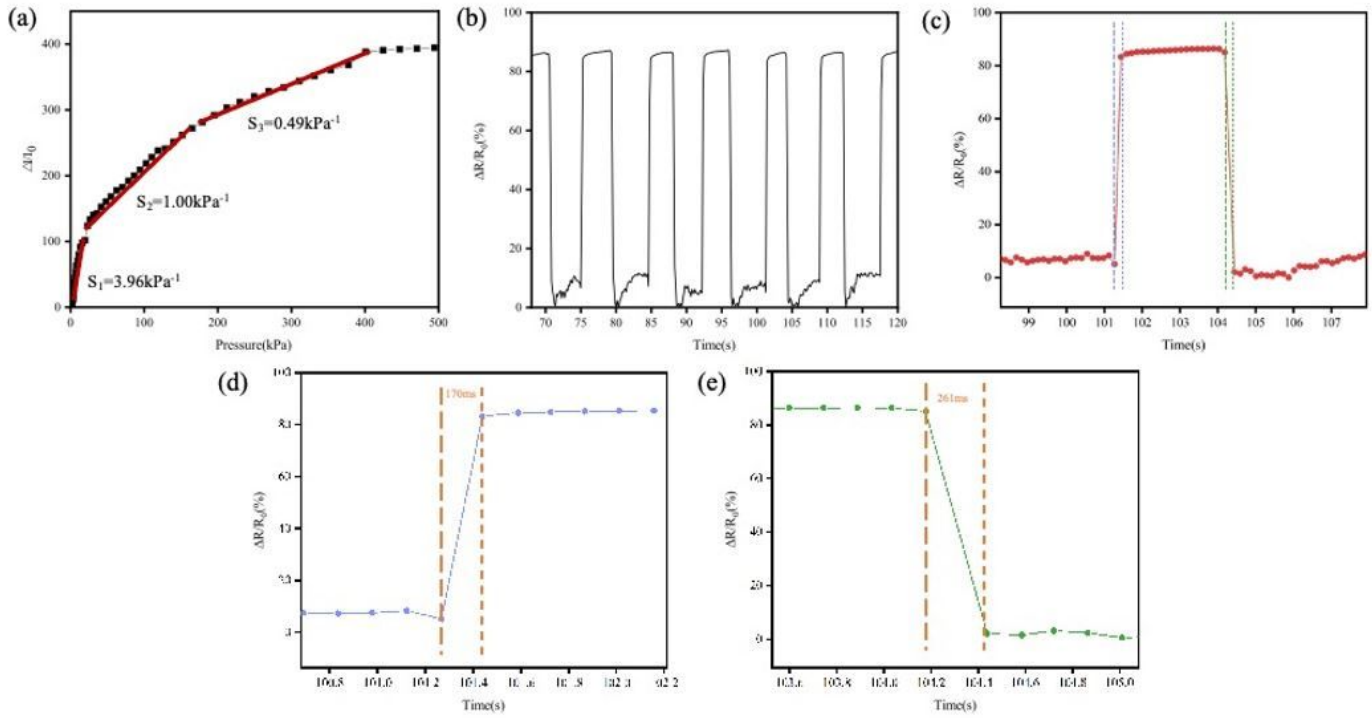

Figure 3

(a) The sensitivity performace of TPRS. (b) Real-time response of the sensor under an applied pressure of 5 KPa. (c) Pressure response showing a single cycle, and the corresponding (d) response time and (e) releasing time.

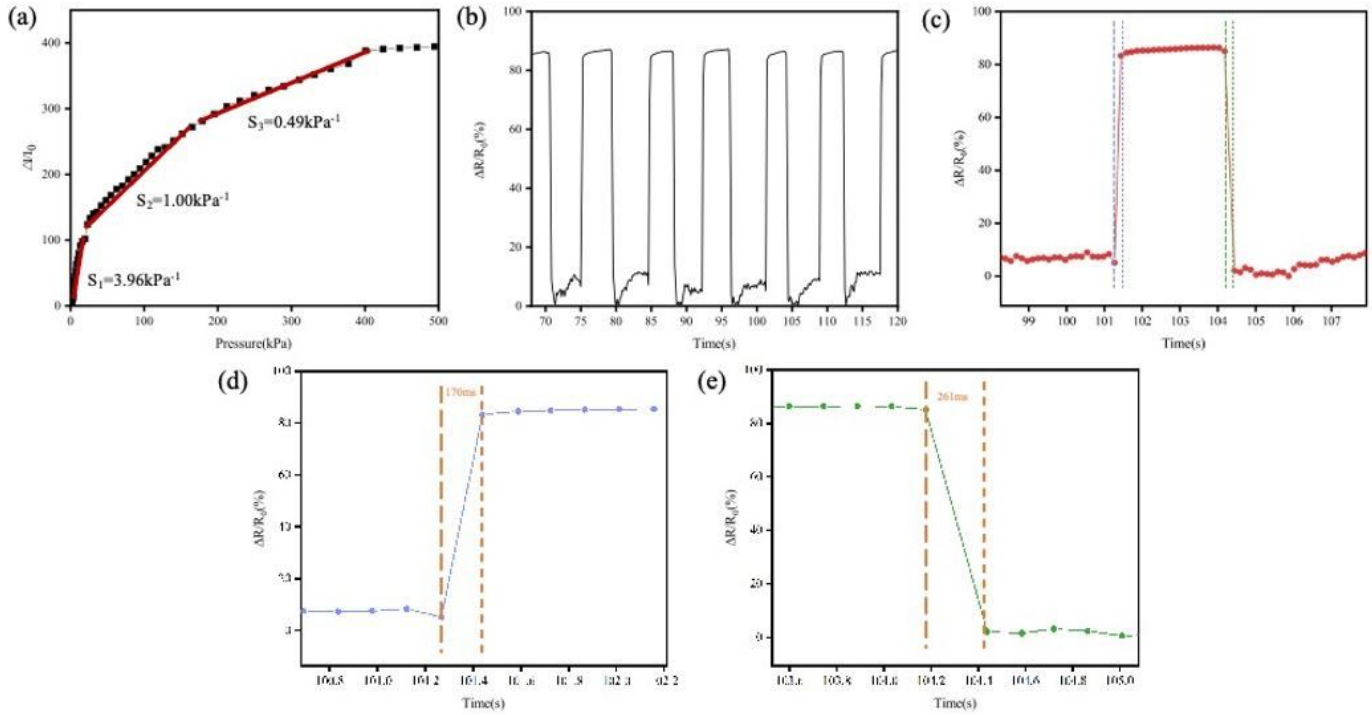

Figure 3

(a) The sensitivity performace of TPRS. (b) Real-time response of the sensor under an applied pressure of 5 KPa. (c) Pressure response showing a single cycle, and the corresponding (d) response time and (e) releasing time.

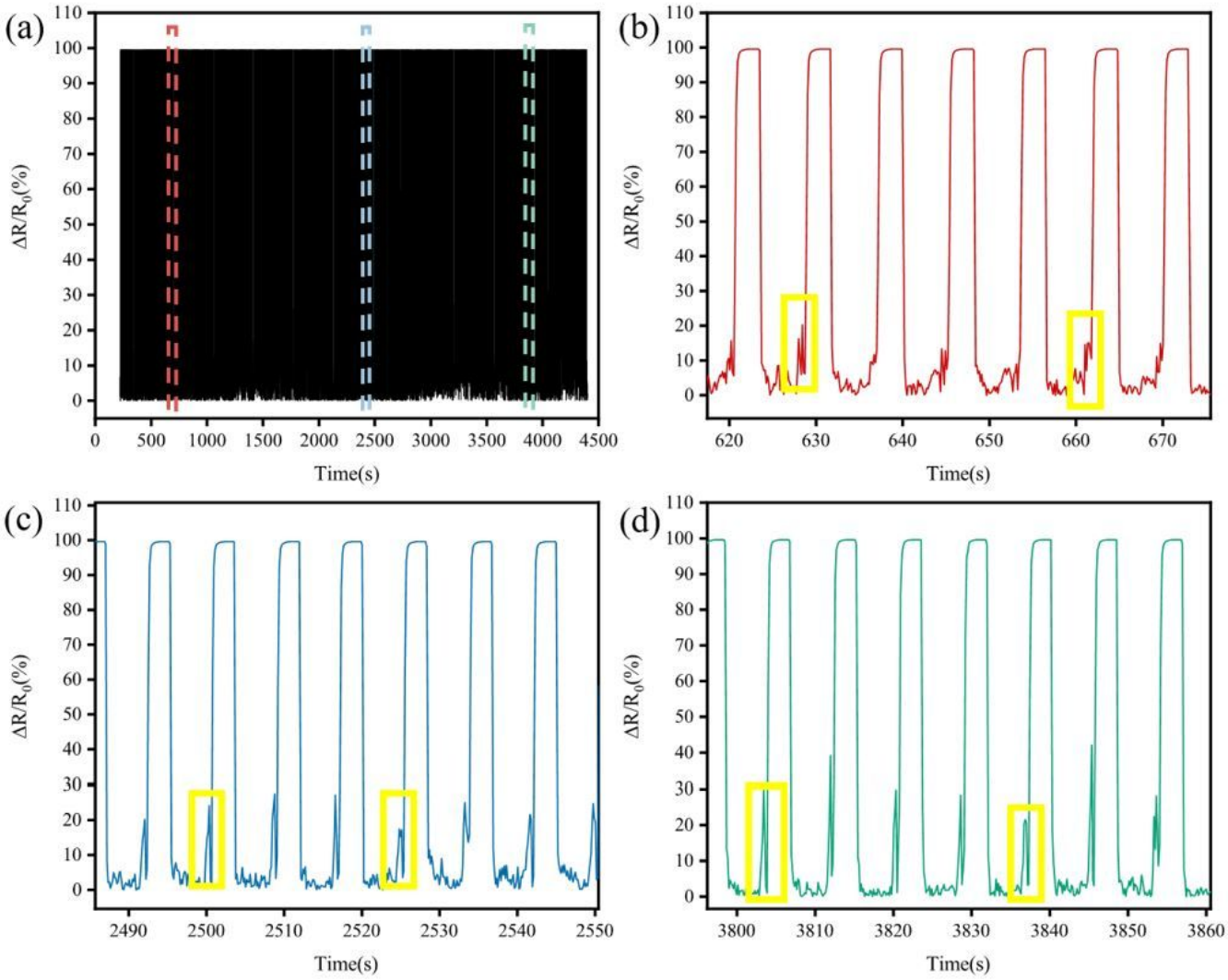

Figure 4

(a) The TPRS durability test (1000 cycles), (b) The enlarged view of the red area of (a), (c) The enlarged view of the blue area of (a), (d) The enlarged view of the green area of (a).

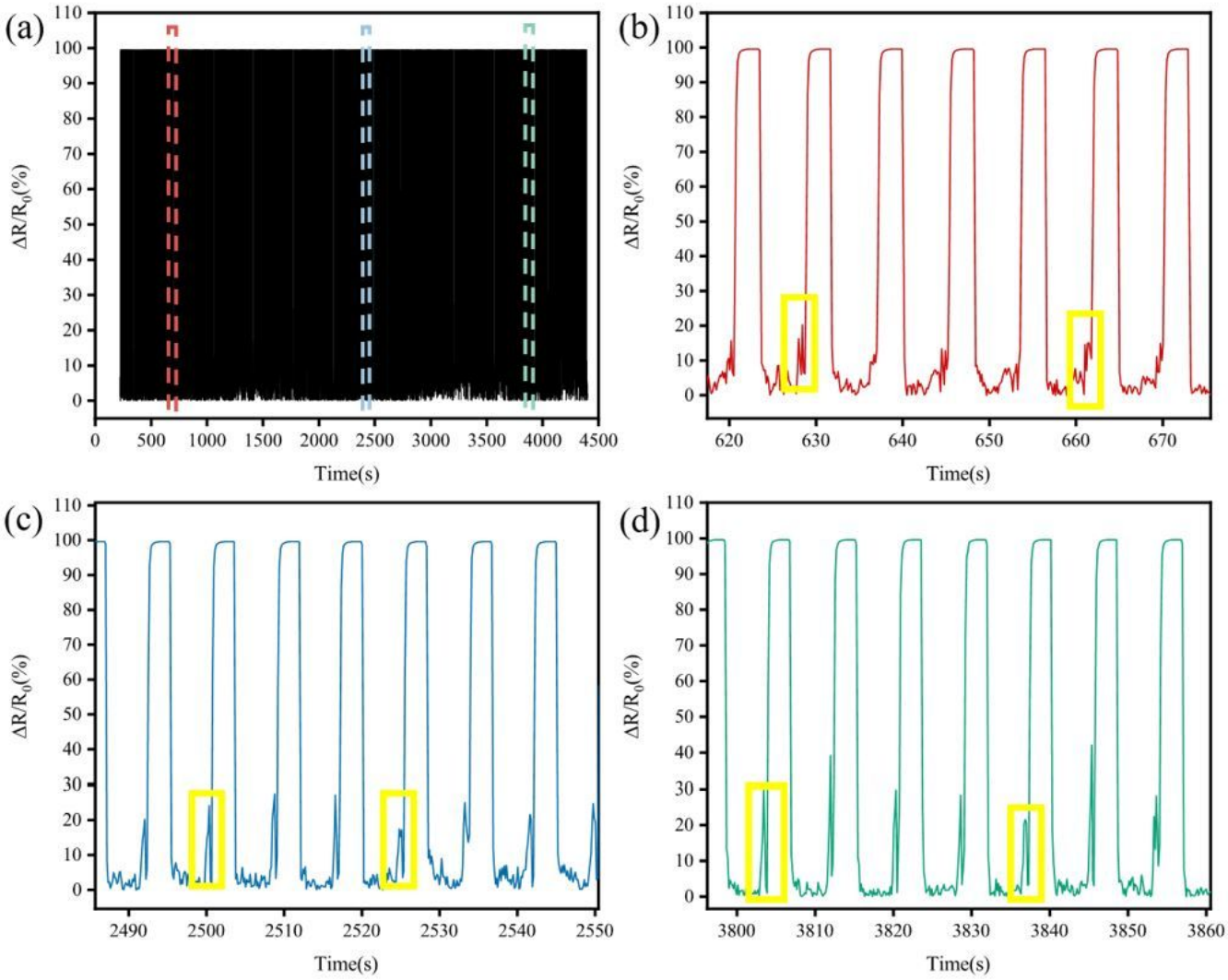

Figure 4

(a) The TPRS durability test (1000 cycles), (b) The enlarged view of the red area of (a), (c) The enlarged view of the blue area of (a), (d) The enlarged view of the green area of (a).

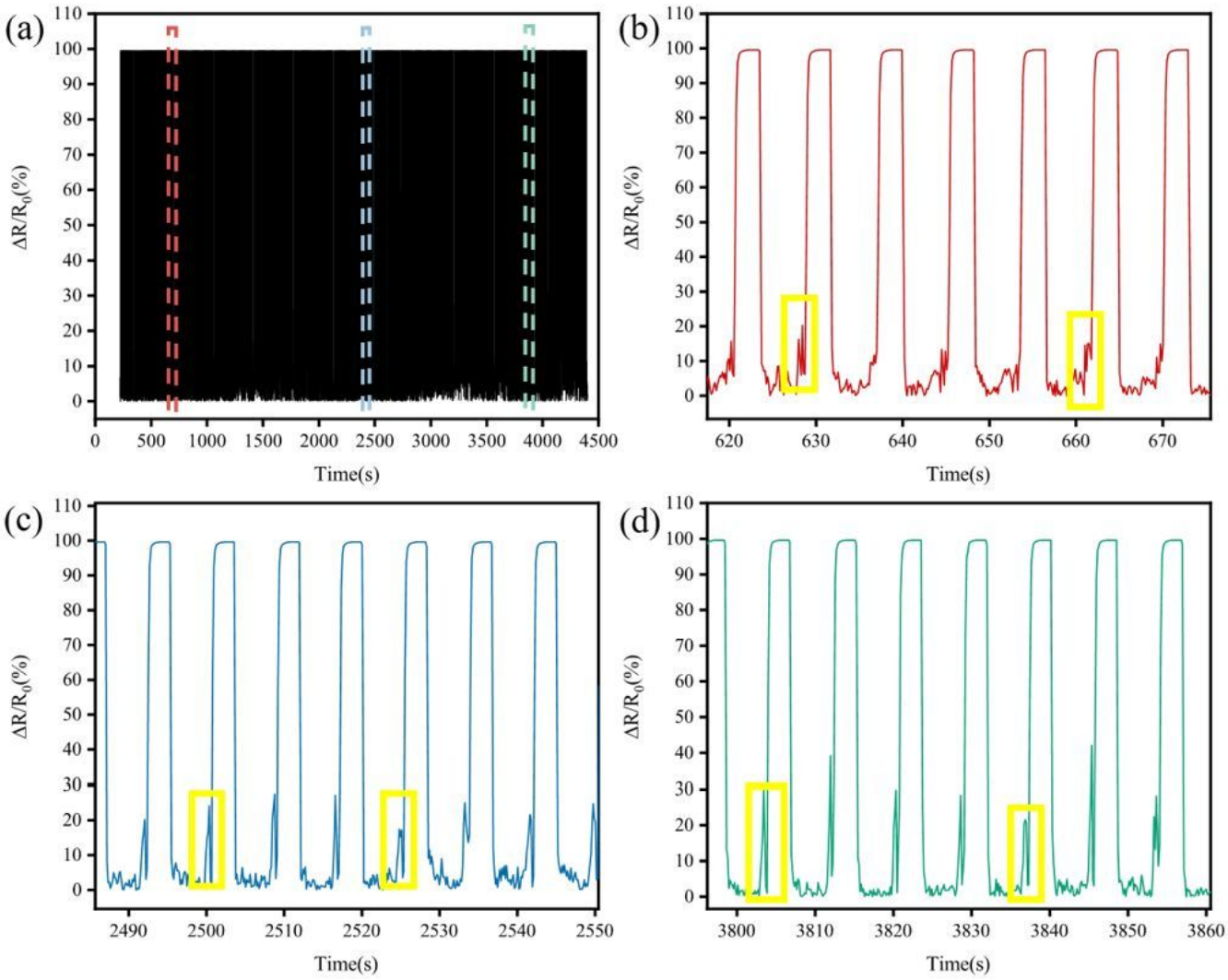

Figure 4

(a) The TPRS durability test (1000 cycles), (b) The enlarged view of the red area of (a), (c) The enlarged view of the blue area of (a), (d) The enlarged view of the green area of (a).

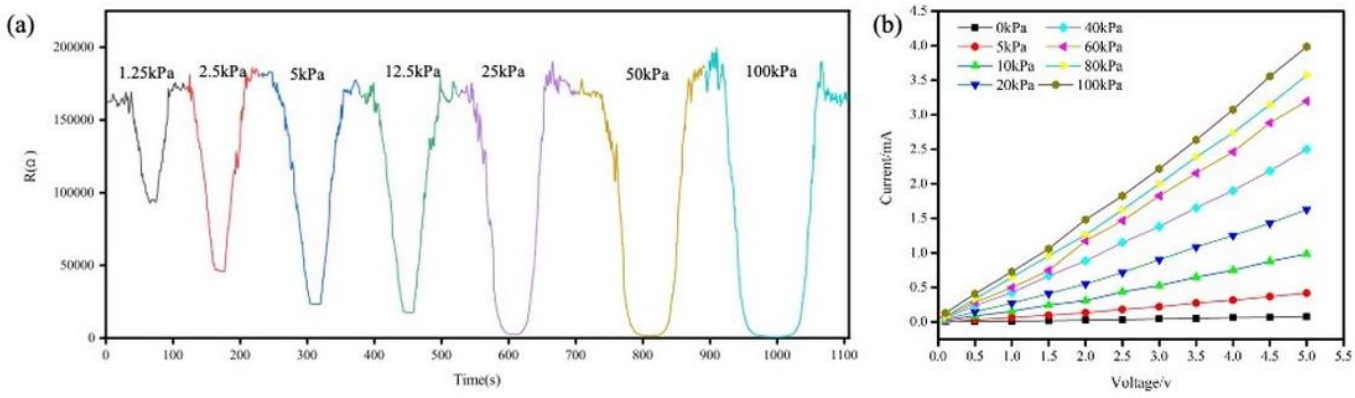

Figure 5

(a) Relative electrical resistance changes under different pressure. (b) The relationship between voltage and current.

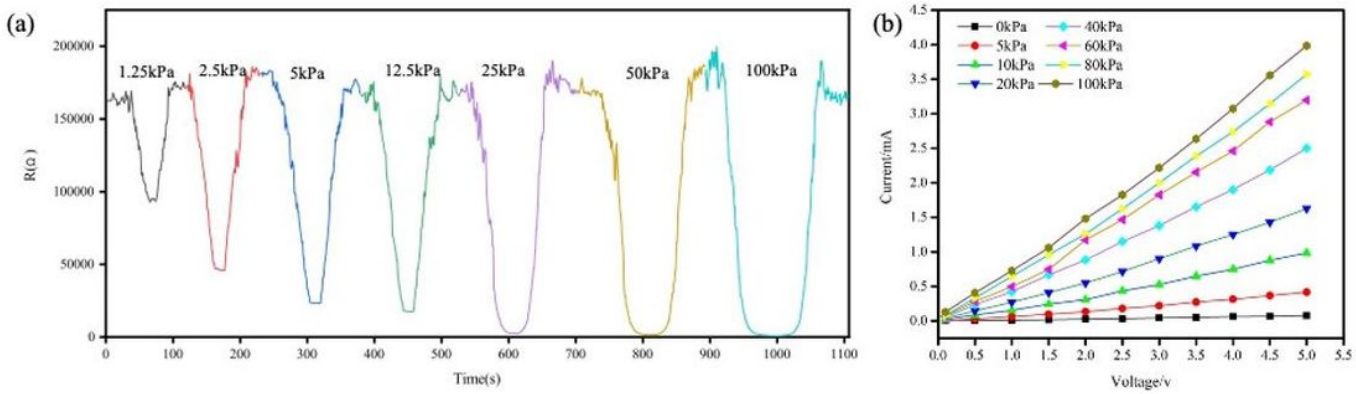

Figure 5

(a) Relative electrical resistance changes under different pressure. (b) The relationship between voltage and current.

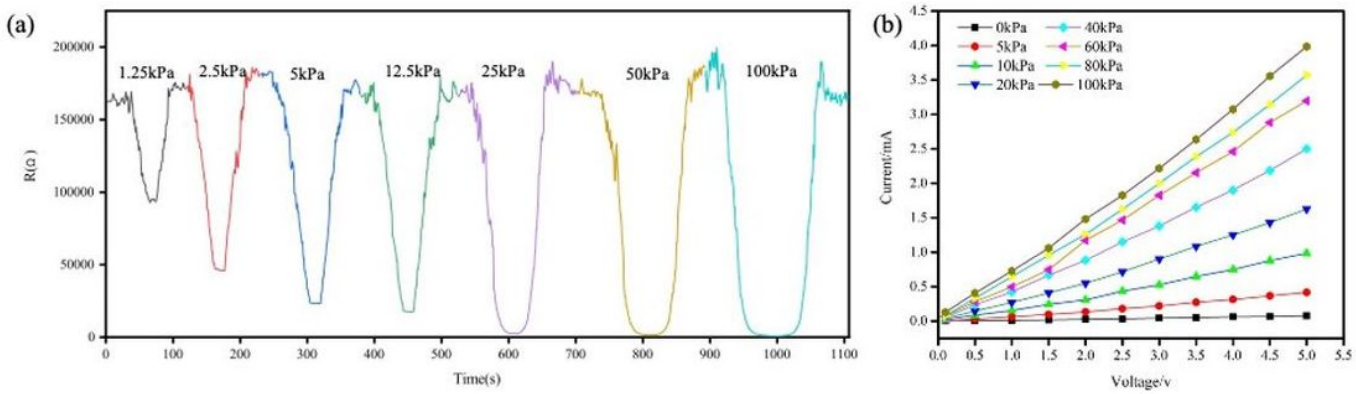

Figure 5

(a) Relative electrical resistance changes under different pressure. (b) The relationship between voltage and current.

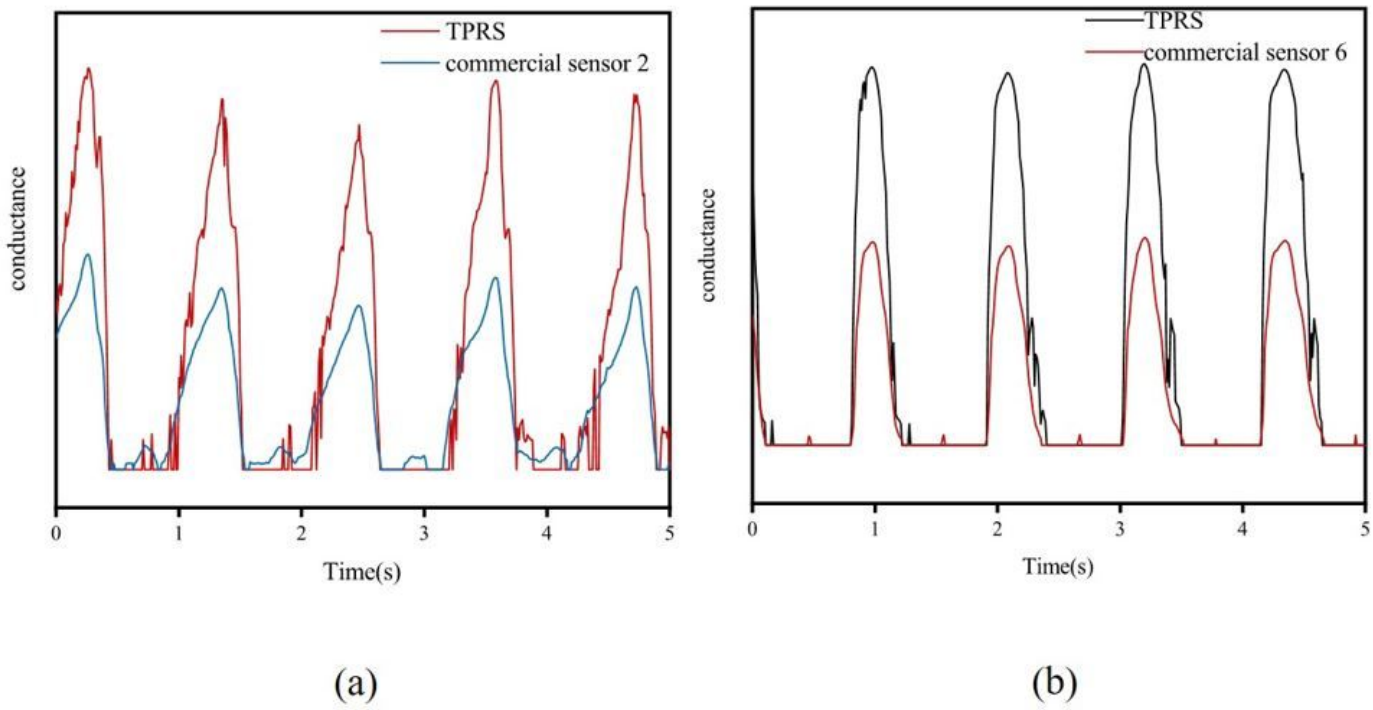

Figure 6

(a) commercial sensor placed over TPRS; (b) signals of sensor 2 and TPRS; (c) signals of sensor 6 and TPRS.

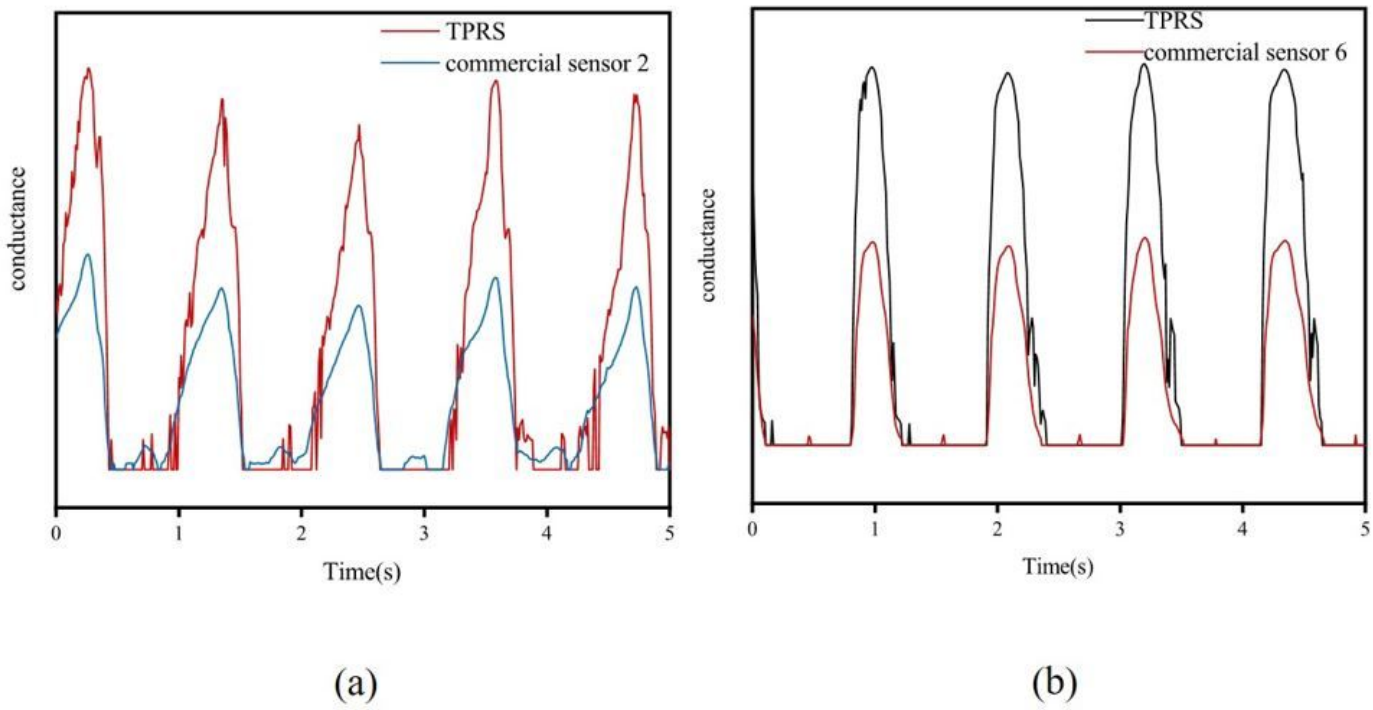

Figure 6

(a) commercial sensor placed over TPRS; (b) signals of sensor 2 and TPRS; (c) signals of sensor 6 and TPRS.

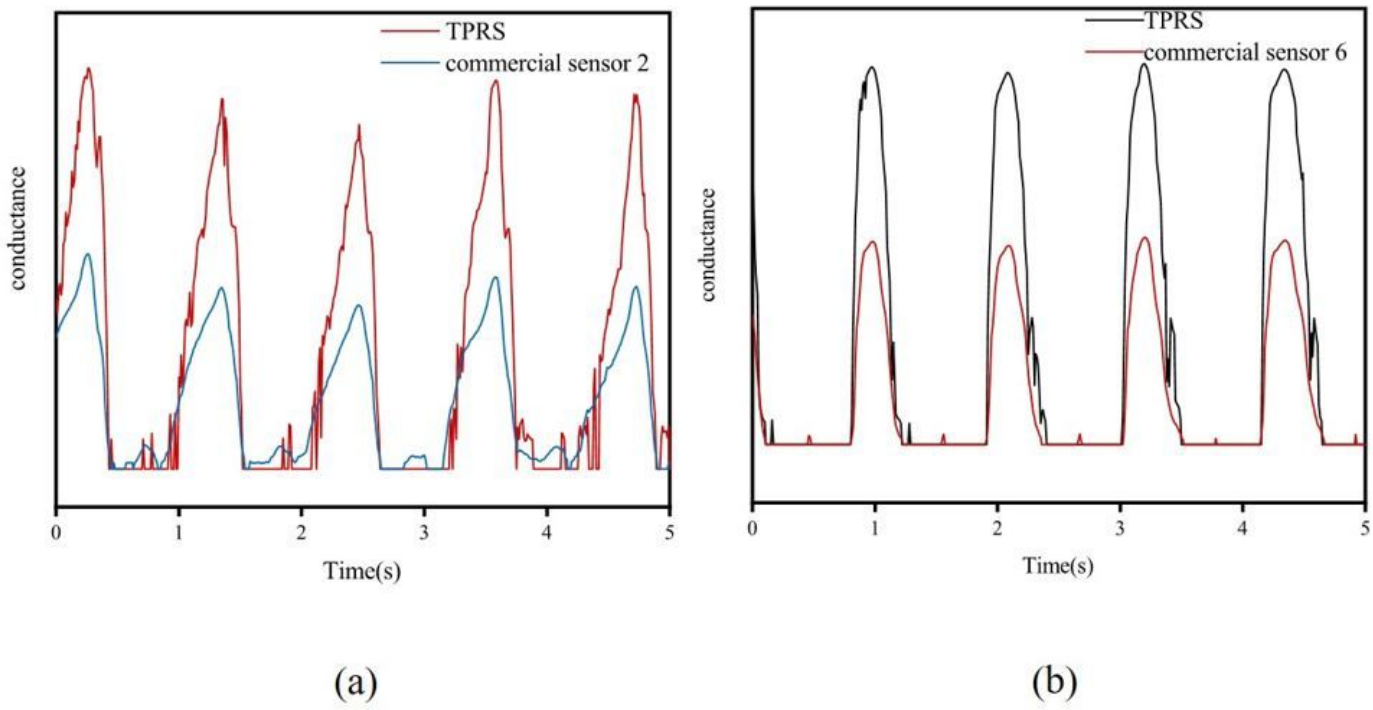

Figure 6

(a) commercial sensor placed over TPRS; (b) signals of sensor 2 and TPRS; (c) signals of sensor 6 and TPRS.

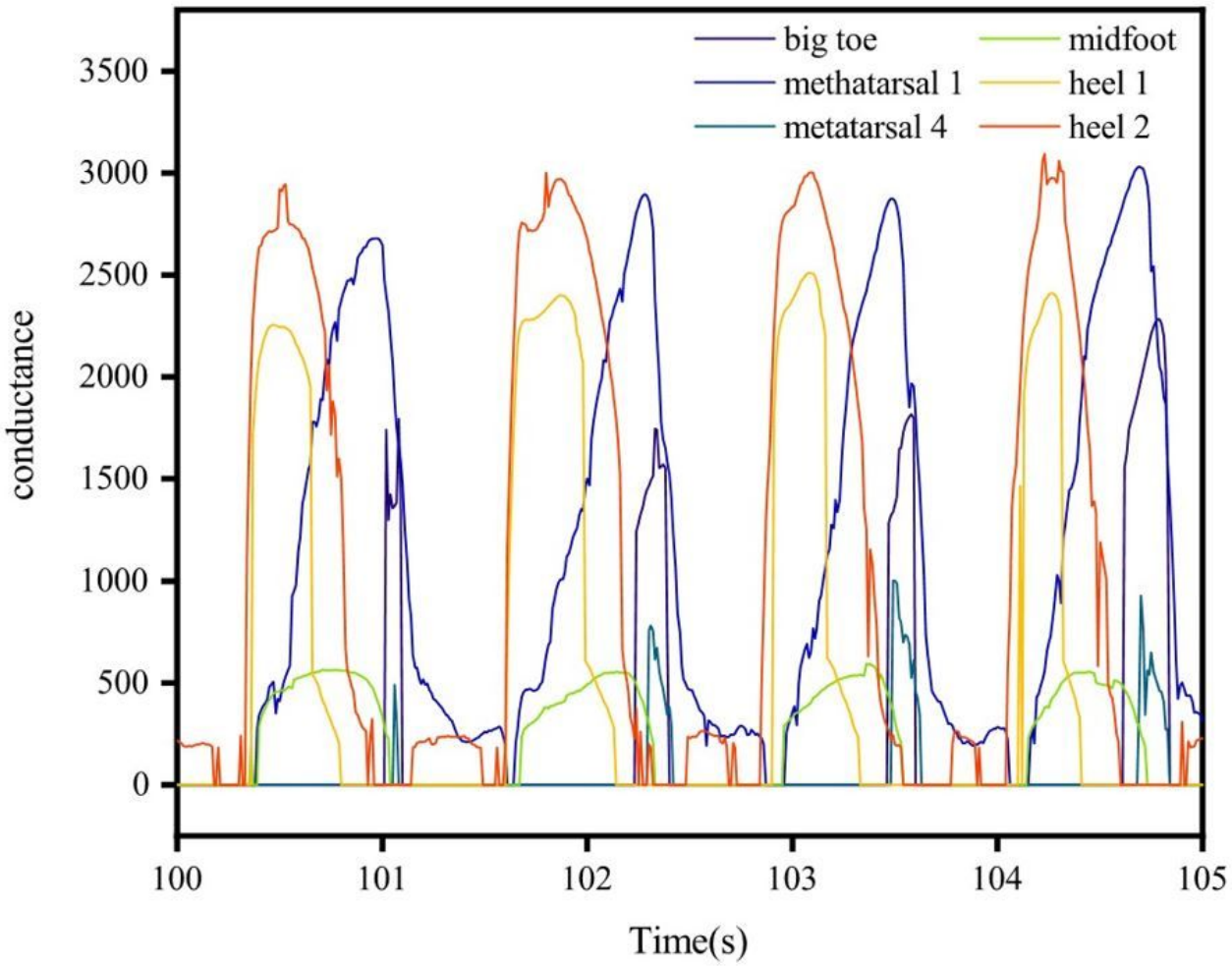

Figure 7

gait cycles reflected by the signals of the designed insole

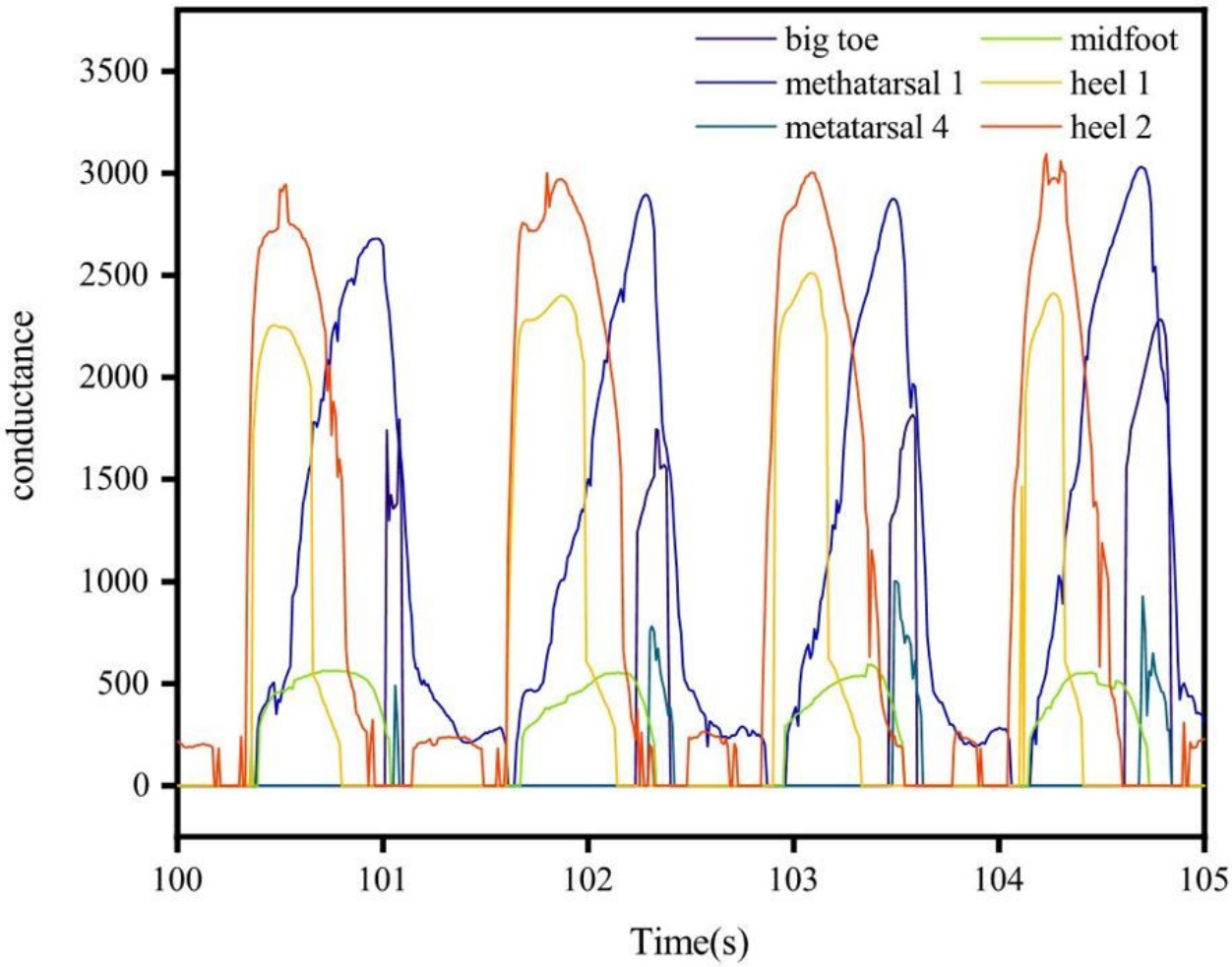

Figure 7

gait cycles reflected by the signals of the designed insole

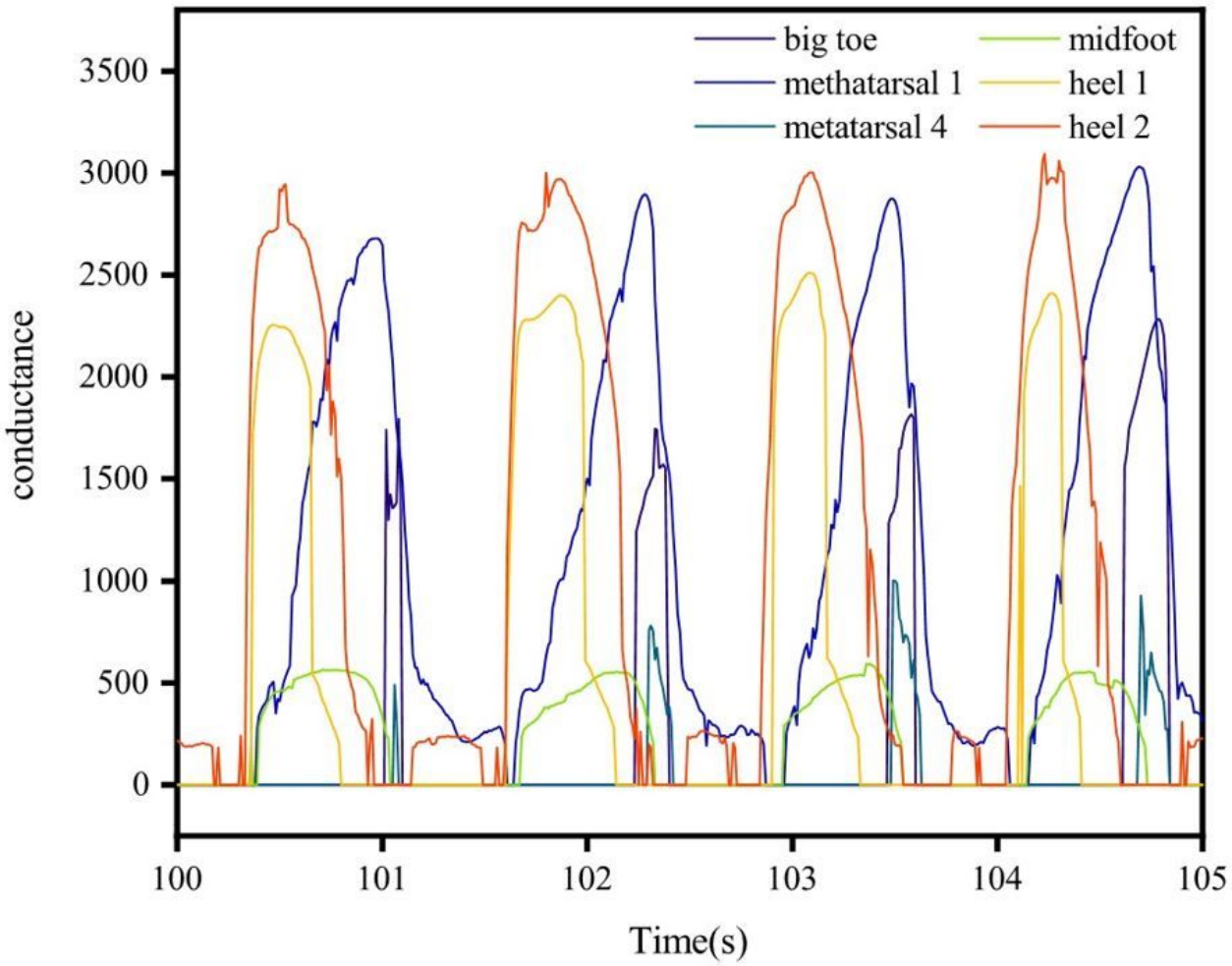

Figure 7

gait cycles reflected by the signals of the designed insole

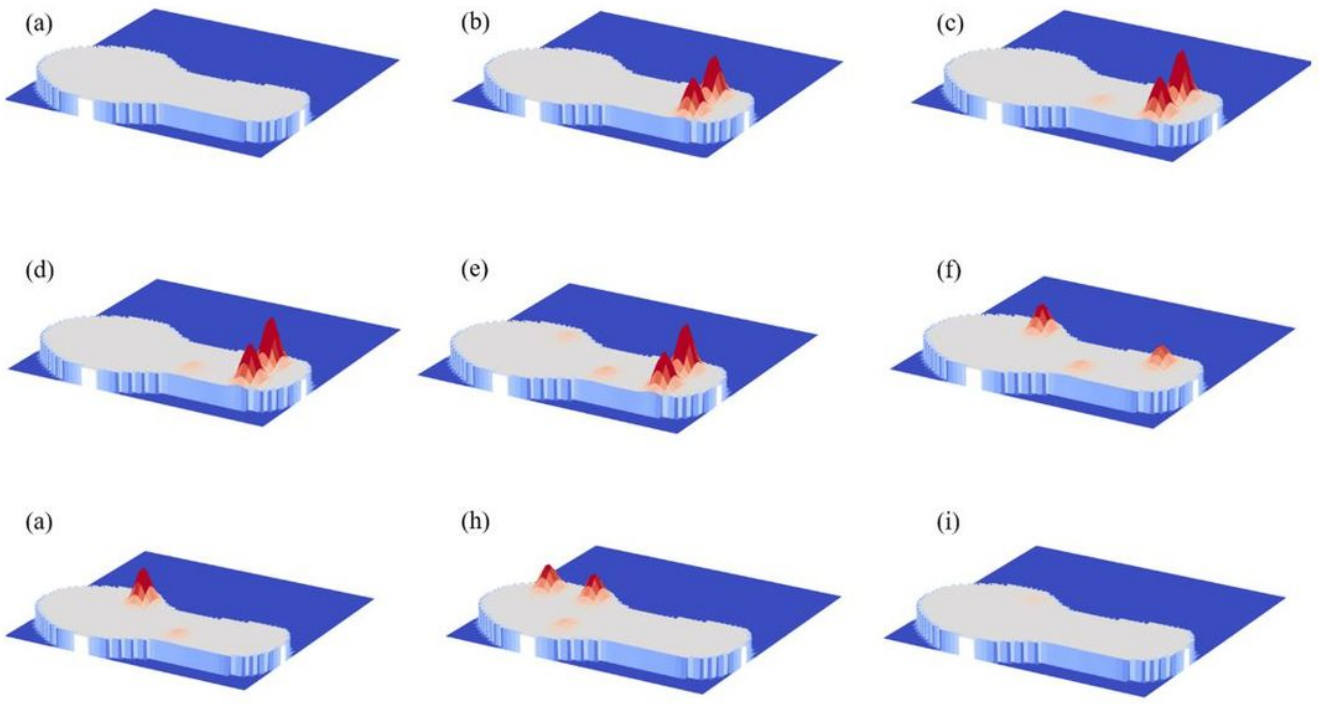

Figure 8

Pressure maps under the foot at different gait phases: (a) feet off the ground, (b)-(d) feet start to land, (e) feet on the ground, (f)-(h) feet start to get off the ground, (i) feet off the ground

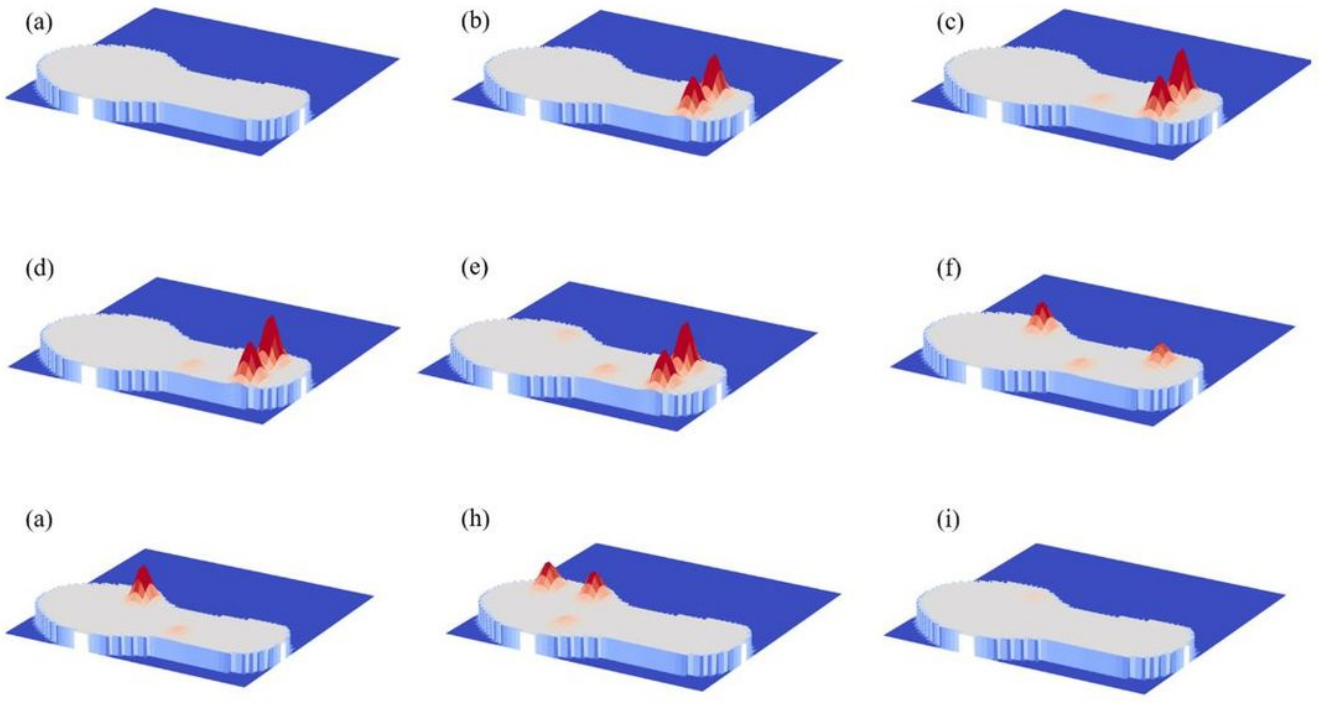

Figure 8

Pressure maps under the foot at different gait phases: (a) feet off the ground, (b)-(d) feet start to land, (e) feet on the ground, (f)-(h) feet start to get off the ground, (i) feet off the ground

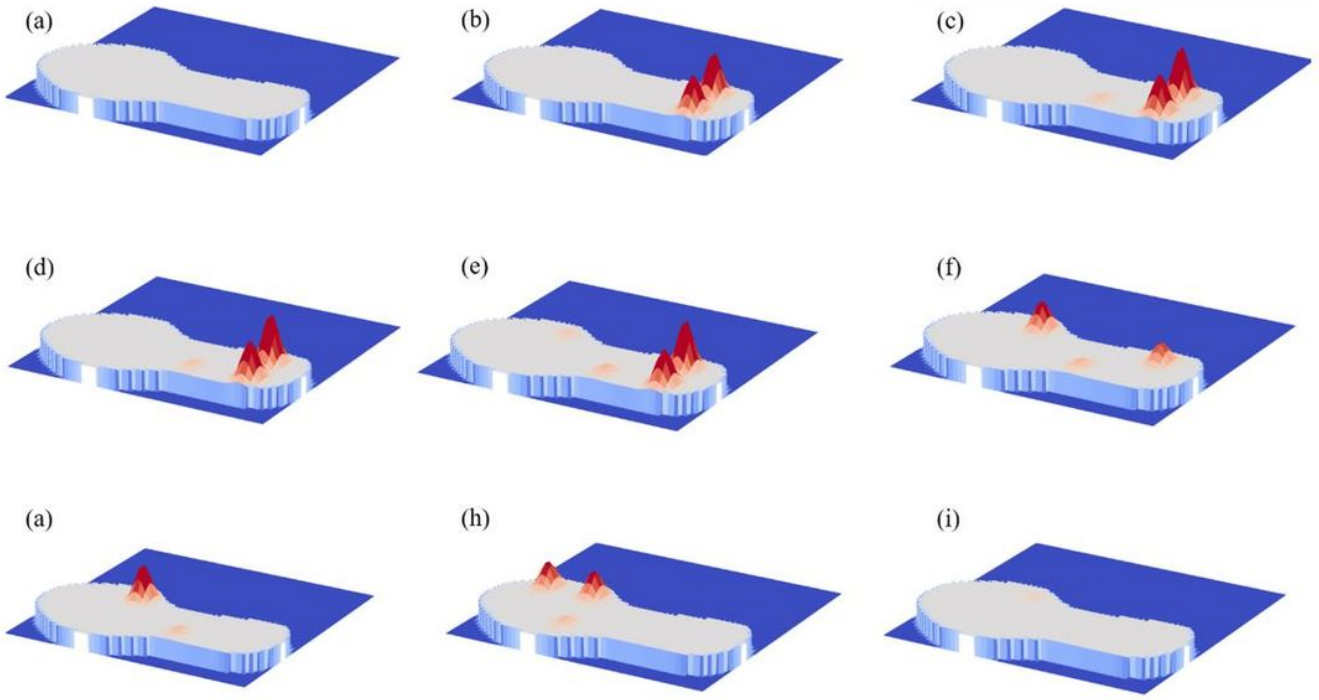

Figure 8

Pressure maps under the foot at different gait phases: (a) feet off the ground, (b)-(d) feet start to land, (e) feet on the ground, (f)-(h) feet start to get off the ground, (i) feet off the ground

Supplementary Files

This is a list of supplementary files associated with this preprint. Click to download.

- FiguremovieS1.mp4
- FiguremovieS1.mp4
- FiguremovieS1.mp4
- SupportingInformatin.docx
- SupportingInformatin.docx
- SupportingInformatin.docx